

REPORT DOCUMENTATION PAGE			Form Approved OMB NO. 0704-0188		
<p>The public reporting burden for this collection of information is estimated to average 1 hour per response, including the time for reviewing instructions, searching existing data sources, gathering and maintaining the data needed, and completing and reviewing the collection of information. Send comments regarding this burden estimate or any other aspect of this collection of information, including suggestions for reducing this burden, to Washington Headquarters Services, Directorate for Information Operations and Reports, 1215 Jefferson Davis Highway, Suite 1204, Arlington VA, 22202-4302. Respondents should be aware that notwithstanding any other provision of law, no person shall be subject to any penalty for failing to comply with a collection of information if it does not display a currently valid OMB control number.</p> <p>PLEASE DO NOT RETURN YOUR FORM TO THE ABOVE ADDRESS.</p>					
1. REPORT DATE (DD-MM-YYYY) 31-03-2011		2. REPORT TYPE Final Report		3. DATES COVERED (From - To) 1-Jul-2007 - 31-Dec-2010	
4. TITLE AND SUBTITLE Nanoscale Deformation and Toughening Mechanisms of Nacre			5a. CONTRACT NUMBER W911NF-07-1-0449		
			5b. GRANT NUMBER		
			5c. PROGRAM ELEMENT NUMBER 611102		
6. AUTHORS Xiaodong Li			5d. PROJECT NUMBER		
			5e. TASK NUMBER		
			5f. WORK UNIT NUMBER		
7. PERFORMING ORGANIZATION NAMES AND ADDRESSES University of South Carolina Office of Sponsored Programs & Research James F. Byrnes International Center Columbia, SC 29208 -			8. PERFORMING ORGANIZATION REPORT NUMBER		
9. SPONSORING/MONITORING AGENCY NAME(S) AND ADDRESS(ES) U.S. Army Research Office P.O. Box 12211 Research Triangle Park, NC 27709-2211			10. SPONSOR/MONITOR'S ACRONYM(S) ARO		
			11. SPONSOR/MONITOR'S REPORT NUMBER(S) 52705-MS.3		
12. DISTRIBUTION AVAILABILITY STATEMENT Approved for Public Release; Distribution Unlimited					
13. SUPPLEMENTARY NOTES The views, opinions and/or findings contained in this report are those of the author(s) and should not be construed as an official Department of the Army position, policy or decision, unless so designated by other documentation.					
14. ABSTRACT We found direct evidence that a single-crystal-like aragonite platelet is essentially assembled with aragonite nanoparticles. The aragonite nanoparticles are readily oriented and assembled into pseudo-single-crystal aragonite platelets via screw dislocation and amorphous aggregation, which are two dominant mediating mechanisms between nanoparticles during biomineralization. The heat treatment burned out the biopolymer in nacre, leaving nanoscale holes at the aragonite platelet boundaries and on the platelet surfaces. By directly probing the biopolymer					
15. SUBJECT TERMS Seashell; Nacre; Aragonite; Biopolymer; Deformation; Strength; Toughness; Impact loading; Mechanical properties; Deformation strengthening					
16. SECURITY CLASSIFICATION OF:			17. LIMITATION OF ABSTRACT UU	15. NUMBER OF PAGES	19a. NAME OF RESPONSIBLE PERSON Xiaodong Li
a. REPORT UU	b. ABSTRACT UU	c. THIS PAGE UU			19b. TELEPHONE NUMBER 803-777-8011

Report Title

Nanoscale Deformation and Toughening Mechanisms of Nacre

ABSTRACT

We found direct evidence that a single-crystal-like aragonite platelet is essentially assembled with aragonite nanoparticles. The aragonite nanoparticles are readily oriented and assembled into pseudo-single-crystal aragonite platelets via screw dislocation and amorphous aggregation, which are two dominant mediating mechanisms between nanoparticles during biomineralization. The heat treatment burned out the biopolymer in nacre, leaving nanoscale holes at the aragonite platelet boundaries and on the platelet surfaces. By directly probing the biopolymer nanostrands using an atomic force microscope, we unveiled that the biopolymer in nacre has the capability to strengthen itself during deformation. An elastic modulus of 10.57 GPa was determined for nacre biopolymer matrix for the first time. Under high strain rate compression, nacre exhibits surprisingly high fracture strength and relatively marked plastic deformation excursion compared with those in the quasi-static loading mode. We discovered a new deformation mechanism that the emission of partial dislocation and the onset of deformation twinning jointly play a dominated role in the increased fracture strength and ductility. This project has supported 1 postdoctoral researcher and 3 PhD students. Five papers have been published or submitted for publication in prestigious referred journals. The work has been presented at 16 international conferences.

List of papers submitted or published that acknowledge ARO support during this reporting period. List the papers, including journal references, in the following categories:

(a) Papers published in peer-reviewed journals (N/A for none)

Xiaodong Li and Zaiwang Huang, "Unveiling the Formation Mechanism of Pseudo-Single Crystal Aragonite Platelets in Nacre," Physical Review Letters, 102 (2009) 075502.

Zaiwang Huang and Xiaodong Li, "Nanoscale Structural and Mechanical Characterization of Heat Treated Nacre," Materials Science and Engineering C, 29 (2009) 1803-1807.

Number of Papers published in peer-reviewed journals: 2.00

(b) Papers published in non-peer-reviewed journals or in conference proceedings (N/A for none)

Number of Papers published in non peer-reviewed journals: 0.00

(c) Presentations

Xiaodong Li, "Unveiling the Strengthening and Toughening Mechanisms of Nacre - Lessons from Nature," 2011 ASME Annual Conference, International Mechanical Engineering Congress & Exposition (IMECE), Denver, Colorado, November 11- 17, 2011 (invited keynote).

Xiaodong Li, "Unveiling Deformation and Toughening Mechanisms of Nacre," 35th International Conference and Exposition on Advanced Ceramics and Composites (ICACC'11), Daytona Beach, Florida, January 23-28, 2011 (invited).

Xiaodong Li, "Deformation and Toughening Mechanisms of Natural Biological Nanocomposites - Lessons from Nature," 3rd International Conference on One-dimensional Nanomaterials (ICON 2009), Atlanta, Georgia, December 7- 9, 2009 (invited).

Xiaodong Li and Zaiwang Huang, "Unveiling the Formation Mechanism of Pseudo Single-Crystal Aragonite Platelets in Nacre," MS&T'09, Material Science & Technology 2009 Conference & Exhibition, Pittsburgh, PA, October 25-29, 2009 (invited).

Xiaodong Li, "What Roles do Nanostructures Play in the Strengthening and Toughening of Nacre?," MS&T '08, Material Science & Technology 2008 Conference & Exhibition, Pittsburgh, PA, October 5-9, 2008 (invited).

Xiaodong Li, "Nanomechanics of Biological Systems," 2008 MRS Spring Meeting, San Francisco, CA, March 24-28, 2008 (invited).

Xiaodong Li, "Deformation and Toughening Mechanisms of Nanograins - Lessons from Nature," TMS 2008, 137th Annual Meeting & Exhibition, New Orleans, LA, March 9-13, 2008 (invited).

Xiaodong Li, "Deformation and Toughening Mechanisms of Natural Nanocomposites - Lessons from Nature," 32nd International Conference & Exposition on Advanced Ceramics & Composites, Daytona Beach, Florida, January 27-February 1, 2008 (invited).

Haoze Li, Zhi-Hui Xu, and Xiaodong Li, "Nanoscale Structural and Mechanical Characterization of Conch Shells," 2011 ASME Annual Conference, International Mechanical Engineering Congress & Exposition (IMECE), Denver, Colorado, November 11- 17, 2011.

Xiaodong Li, "Unveiling the Deformation and Toughening Mechanisms of Nacre – Lessons from Nature," TMS 2011, 140th Annual Meeting & Exhibition, San Diego, California, February 27 - March 3, 2011.

Xiaodong Li and Zaiwang Huang, "Unveiling the Formation Mechanism of Pseudo Single-Crystal Aragonite Platelets in Nacre," TMS 2010, 139th Annual Meeting & Exhibition, Seattle, WA, February 14-18, 2010.

Xiaodong Li and Zaiwang Huang, "Unveiling the Formation Mechanism of Nanostructured Aragonite Platelets in Nacre," 2009 MRS Fall Meeting, Boston, MA, November 30 – December 4, 2009.

Zaiwang Huang and Xiaodong Li, "Nanoscale Structural and Mechanical Characterization of Heat Treated Natural Nanoparticle-based Material – Nacre," MS&T '09, Materials Science & Technology 2009 Conference & Exhibition, Detroit, Michigan, October 25-29, 2009.

Zaiwang Huang and Xiaodong Li, Temperature Effect on the Structure and Mechanical Properties of Nacre, TMS 2009, 138th Annual Meeting & Exhibition, San Francisco, CA, February 15-19, 2009.

Xiaodong Li, Zhi-Hui Xu, Zaiwang Huang, Wei-Che Chang, Yuh J. Chao, Rizhi Wang, and Min Chang, Deformation and Toughening Mechanisms of Nacre, 2008 ASME Annual Conference, International Mechanical Engineering Congress & Exposition (IMECE), Boston, MA, October 31- November 6, 2008.

Xiaodong Li, Zhi-Hui Xu, Wei-Che Chang, Yuh J. Chao, Rizhi Wang, and Min Chang, Nanoscale Structural and Mechanical Characterization of Nacre, 2008 SEM Annual Conference, Orlando, FL, June 2-5, 2008.

Number of Presentations: 16.00

Non Peer-Reviewed Conference Proceeding publications (other than abstracts):

Number of Non Peer-Reviewed Conference Proceeding publications (other than abstracts):

0

Peer-Reviewed Conference Proceeding publications (other than abstracts):

(d) Manuscripts

Zhi-Hui Xu and Xiaodong Li, "Deformation Strengthening of the Biopolymer Matrix of Nacre," submitted for publication.

Zhi-Hui Xu, Yingchao Yang, Zaiwang Huang, and Xiaodong Li, "Elastic Modulus of Biopolymer Matrix in Nacre Measured Using Coupled Atomic Force Microscopy Bending and Inverse Finite Element Techniques," submitted for publication.

Zaiwang Huang, Haoze Li, Zhiliang Pan, Qiuming Wei, and Xiaodong Li, "New Deformation Mechanism in Nacre," submitted for publication.

Number of Manuscripts: 3.00

Patents Submitted

Patents Awarded

Awards

1. University of South Carolina College of Engineering and Computing Research Progress Award, 2008

2. One keynote and seven invited talks at the international conferences (see below).

Xiaodong Li, "Unveiling the Strengthening and Toughening Mechanisms of Nacre - Lessons from Nature," 2011 ASME Annual Conference, International Mechanical Engineering Congress & Exposition (IMECE), Denver, Colorado, November 11- 17, 2011 (invited keynote).

Xiaodong Li, "Unveiling Deformation and Toughening Mechanisms of Nacre," 35th International Conference and Exposition on Advanced Ceramics and Composites (ICACC'11), Daytona Beach, Florida, January 23-28, 2011 (invited).

Xiaodong Li, "Deformation and Toughening Mechanisms of Natural Biological Nanocomposites - Lessons from Nature," 3rd International Conference on One-dimensional Nanomaterials (ICON 2009), Atlanta, Georgia, December 7- 9, 2009 (invited).

Xiaodong Li and Zaiwang Huang, "Unveiling the Formation Mechanism of Pseudo Single-Crystal Aragonite Platelets in Nacre," MS&T'09, Material Science & Technology 2009 Conference & Exhibition, Pittsburgh, PA, October 25-29, 2009 (invited).

Xiaodong Li, "What Roles do Nanostructures Play in the Strengthening and Toughening of Nacre?," MS&T '08, Material Science & Technology 2008 Conference & Exhibition, Pittsburgh, PA, October 5-9, 2008 (invited).

Xiaodong Li, "Nanomechanics of Biological Systems," 2008 MRS Spring Meeting, San Francisco, CA, March 24-28, 2008 (invited).

Xiaodong Li, "Deformation and Toughening Mechanisms of Nanograins - Lessons from Nature," TMS 2008, 137th Annual Meeting & Exhibition, New Orleans, LA, March 9-13, 2008 (invited).

Xiaodong Li, "Deformation and Toughening Mechanisms of Natural Nanocomposites - Lessons from Nature," 32nd International Conference & Exposition on Advanced Ceramics & Composites, Daytona Beach, Florida, January 27-February 1, 2008 (invited).

3. Invited to serve on the following three editorial boards.

Editorial Board, International Journal of Applied Mechanics

Editorial Board, Journal of Biomaterials and Nanobiotechnology

Editorial Board, Journal of Nanoscience Letters

4. Guest editors for the following journal special issues.

Guest Editor, Experimental Mechanics, Special Issue - Advanced Vision Based Methods and Measurements

Guest Editor, Experimental Mechanics, Special Issue - Emerging Methods to Understand Mechanical Behavior

Guest Editor, Metallurgical and Materials Transactions A, Special Issue - Mechanical Behavior of Nanostructured Materials

Guest Editor, JOM – Nanomechanical Testing

5. Chairman of the TMS - Nanomechanical Materials Behavior Committee

Graduate Students

<u>NAME</u>	<u>PERCENT SUPPORTED</u>
Yong Sun	0.25
Zaiwang Huang	0.50
Haoze	0.25
FTE Equivalent:	1.00
Total Number:	3

Names of Post Doctorates

<u>NAME</u>	<u>PERCENT SUPPORTED</u>
Zhi-Hui Xu	1.00
FTE Equivalent:	1.00
Total Number:	1

Names of Faculty Supported

<u>NAME</u>	<u>PERCENT SUPPORTED</u>	National Academy Member
Xiaodong Li	0.10	No
FTE Equivalent:	0.10	
Total Number:	1	

Names of Under Graduate students supported

<u>NAME</u>	<u>PERCENT SUPPORTED</u>
FTE Equivalent:	
Total Number:	

Student Metrics

This section only applies to graduating undergraduates supported by this agreement in this reporting period

- The number of undergraduates funded by this agreement who graduated during this period: 0.00
- The number of undergraduates funded by this agreement who graduated during this period with a degree in science, mathematics, engineering, or technology fields:..... 0.00
- The number of undergraduates funded by your agreement who graduated during this period and will continue to pursue a graduate or Ph.D. degree in science, mathematics, engineering, or technology fields:..... 0.00
- Number of graduating undergraduates who achieved a 3.5 GPA to 4.0 (4.0 max scale):..... 0.00
- Number of graduating undergraduates funded by a DoD funded Center of Excellence grant for Education, Research and Engineering: 0.00
- The number of undergraduates funded by your agreement who graduated during this period and intend to work for the Department of Defense 0.00
- The number of undergraduates funded by your agreement who graduated during this period and will receive scholarships or fellowships for further studies in science, mathematics, engineering or technology fields: 0.00

Names of Personnel receiving masters degrees

<u>NAME</u>
Total Number:

Names of personnel receiving PHDs

<u>NAME</u>
Total Number:

Names of other research staff

NAME

PERCENT SUPPORTED

FTE Equivalent:

Total Number:

Sub Contractors (DD882)

Inventions (DD882)

Scientific Progress

We found direct evidence that a single-crystal-like aragonite platelet is essentially assembled with aragonite nanoparticles. The aragonite nanoparticles are readily oriented and assembled into pseudosingle-crystal aragonite platelets via screw dislocation and amorphous aggregation, which are two dominant mediating mechanisms between nanoparticles during biomineralization. These findings will advance our understanding of nacre's biomineralization process and provide additional design guidelines for developing biomimetic materials.

Nanoscale structural and mechanical characterization of heat treated nacre has been carried out. Two phase transformations were identified, i.e., from aragonite to calcite in the 500 °C heat treated nacre and from aragonite to calcium oxide (CaO) in the 1000 °C heat treated nacre. The brick-mortar architecture remains in the 500 °C heat treated nacre, but loses in the 1000 °C heat treated nacre. The heat treatment burned out the biopolymer in nacre. Nanoscale holes were discovered at the aragonite platelet boundaries and on the platelet surfaces. The heat treated nacre exhibits a sharp loss in elastic modulus and hardness compared with the fresh nacre.

Other than maintaining the integrity of nacre's brick-and-mortar nanoarchitecture, the biopolymer plays a critical role in the strengthening and toughening of nacre. By directly probing the biopolymer nanostrands using an atomic force microscope, we unveiled that the biopolymer in nacre has the capability to strengthen itself during deformation. This unusual deformation strengthening mechanism contributes remarkably to the ultra-high toughness of nacre, which can be explained by a coil spring model. The findings advance the understanding of the mystery of nacre's toughening mechanisms, provide additional design guidelines for developing biomimetic nanomaterials, and lay a constitutive foundation for modeling the deformation behavior of nacre.

A novel approach combining atomic force microscopy probing of nacre biopolymer strand and inverse finite element analysis has been used to directly measure the elastic modulus of nacre biopolymer matrix. An elastic modulus of 10.57 GPa was determined for nacre biopolymer matrix for the first time from the direct measurement. This property is essential for a fundamental understanding of the roles that the biopolymer matrix plays in nacre's strengthening and toughening, and provides guidelines in selecting engineering polymers for biomimetic materials design and fabrication. Such coupled experimental and modeling techniques should find more applications in studying the mechanical behavior of biological materials.

Under high strain rate compression, nacre exhibits surprisingly high fracture strength and relatively marked plastic deformation excursion compared with those in the quasi-static loading mode. We discovered a new deformation mechanism, adopted by natural nacre to protect from predatory penetrating impacts, that the emission of partial dislocation and the onset of deformation twinning jointly play a dominated role in the increased fracture strength and ductility. Our findings have provided solid evidence that Mother Nature delicately uses design principle down to atomic scale with a purpose to fight against foreign attacks, which has opened up a new opportunity to unravel the deformation mechanism of unique mechanical performance at the atomic scale.

Technology Transfer

Nanoscale Deformation and Toughening Mechanisms of Nacre

Professor Xiaodong Li
Department of Mechanical Engineering
University of South Carolina
300 Main Street
Columbia, SC 29208
Phone: 803-777-8011
Fax: 803-777-0106
Email: lixiao@engr.sc.edu

Table of Contents

1. Foreword.....	Page 1
2. Statement of the problem studied	Page 2
3. Summary of the most important results	Page 2
4. Bibliography.....	Page 3
5. Appendixes	Page 4

1. Forward

Armors must be as lightweight as possible while providing sufficient armor protection against the small arms, indirect fire, and mine threats that they are likely to face in combat. Lightweight ceramics have largely failed to fulfill their promise of revolutionizing armors with light strong materials that withstand very high temperature [1,2]. Nacre (mother-of-pearl) is the best example of a natural armor material that exhibits structural robustness, despite the brittle nature of their ceramic constituents. What roles do the nanoscale structures play in the inelasticity and toughening of nacre? Can we learn from this to produce man-made nacre-like armor materials? Existing toughening mechanisms as well as simulation and computational studies, however, cannot explain entirely the high toughness of nacre. This suggests that there are unrevealed structural and toughening secrets that additionally contribute to the toughness of nacre [3]. A systematic study on the nanoscale deformation and toughening mechanisms of nacre is anticipated to impact a broad range of fields related to the development of materials for army applications, revolutionize the way of preparing lightweight and super-tough armor materials and structural components, and open up new application opportunities of other materials. Furthermore, the research is well-positioned to capitalize on bio-inspired materials concepts, as well as transfer the new technologies to Army industry partners for exploitation in service

2. Statement of the problem studied

With the support from Army Research Office, The principal investigator (PI) studied (1) the crystal structure and texture of individual aragonite platelets and aragonite nanoparticles, (2) the mechanical properties of individual platelets and the biopolymer between the platelets, (3) nacre's impact loading resistance, and (4) the load transfer mechanisms among the platelets, nanoparticles and biopolymer.

3. Summary of the most important results

With the support from Army Research Office, the PI systematically studied how the nanoscale structures control nacre's deformation and fracture. The most important results are listed below.

1. We found direct evidence that a single-crystal-like aragonite platelet is essentially assembled with aragonite nanoparticles. The aragonite nanoparticles are readily oriented and assembled into pseudosingle-crystal aragonite platelets via screw dislocation and amorphous aggregation, which are two dominant mediating mechanisms between nanoparticles during biomineralization. These findings will advance our understanding of nacre's biomineralization process and provide additional design guidelines for developing biomimetic materials. The findings have been published in *Physical Review Letters*, 102 (2009) 075502 [4].
2. Nanoscale structural and mechanical characterization of heat treated nacre has been carried out. Two phase transformations were identified, i.e., from aragonite to calcite in the 500 °C heat treated nacre and from aragonite to calcium oxide (CaO) in the 1000 °C heat treated nacre. The brick-mortar architecture remains in the 500 °C heat treated nacre, but loses in the 1000 °C heat treated nacre. The heat treatment burned out the biopolymer in nacre. Nanoscale holes were discovered at the aragonite platelet boundaries and on the platelet surfaces. The heat treated nacre exhibits a sharp loss in elastic modulus and hardness compared with the fresh nacre. The findings have been published in *Materials Science and Engineering C*, 29 (2009) 1803-1807 [5].
3. Other than maintaining the integrity of nacre's brick-and-mortar nanoarchitecture, the biopolymer plays a critical role in the strengthening and toughening of nacre. By directly probing the biopolymer nanostrands using an atomic force microscope, we unveiled that the biopolymer in nacre has the capability to strengthen itself during deformation. This unusual deformation strengthening mechanism contributes remarkably to the ultra-high toughness of nacre, which can be explained by a coil spring model. The findings advance the understanding of the mystery of nacre's toughening mechanisms, provide additional design guidelines for developing biomimetic nanomaterials, and lay a constitutive

foundation for modeling the deformation behavior of nacre. The findings have been submitted for publication [6].

4. A novel approach combining atomic force microscopy probing of nacre biopolymer strand and inverse finite element analysis has been used to directly measure the elastic modulus of nacre biopolymer matrix. An elastic modulus of 10.57 GPa was determined for nacre biopolymer matrix for the first time from the direct measurement. This property is essential for a fundamental understanding of the roles that the biopolymer matrix plays in nacre's strengthening and toughening, and provides guidelines in selecting engineering polymers for biomimetic materials design and fabrication. Such coupled experimental and modeling techniques should find more applications in studying the mechanical behavior of biological materials. The findings have been submitted for publication [7].
5. Under high strain rate compression, nacre exhibits surprisingly high fracture strength and relatively marked plastic deformation excursion compared with those in the quasi-static loading mode. We discovered a new deformation mechanism, adopted by natural nacre to protect from predatory penetrating impacts, that the emission of partial dislocation and the onset of deformation twinning jointly play a dominated role in the increased fracture strength and ductility. Our findings have provided solid evidence that Mother Nature delicately uses design principle down to atomic scale with a purpose to fight against foreign attacks, which has opened up a new opportunity to unravel the deformation mechanism of unique mechanical performance at the atomic scale. The findings have been submitted for publication [8].

4. Bibliography

1. W. J. Clegg, K. Kendall, N. M. Alford, T. W. Button, and J. D. Birchall, A Simple Way to Make Tough Ceramics, *Nature*, 347 (1990) 455-457.
2. C.-A. Wang, Y. Huang, Q. Zan, H. Guo, and S. Cai, Biomimetic Structure Design – A Possible Approach to Change the Brittleness of Ceramics in Nature, *Materials Science and Engineering C*, 11 (2000) 9-12.
3. X. D. Li, Nanoscale Structural and Mechanical Characterization of Natural Nanocomposites: Seashells, *JOM*, 59 (3) (2007) 71-74.
4. X. D. Li and Z. W. Huang, Unveiling the Formation Mechanism of Pseudo-Single Crystal Aragonite Platelets in Nacre, *Physical Review Letters*, 102 (2009) 075502.
5. Z. W. Huang and X. D. Li, Nanoscale Structural and Mechanical Characterization of Heat Treated Nacre, *Materials Science and Engineering C*, 29 (2009) 1803-1807.
6. Z. H. Xu and X. D. Li, Deformation Strengthening of the Biopolymer Matrix of Nacre, submitted for publication.

7. Z. H. Xu, Y. C. Yang, Z. H. and X. D. Li, Elastic Modulus of Biopolymer Matrix in Nacre Measured Using Coupled Atomic Force Microscopy Bending and Inverse Finite Element Techniques, submitted for publication.
8. Z. W. Huang, H. Z. Li, Z. L. Pan, Q. M. Wei, and X. D. Li, New Deformation Mechanism in Nacre, submitted for publication.

5. Appendixes

Attached in the Appendixes are 5 papers resulting from the research.

Unveiling the Formation Mechanism of Pseudo-Single-Crystal Aragonite Platelets in Nacre

Xiaodong Li* and Zaiwang Huang

Department of Mechanical Engineering, University of South Carolina, 300 Main Street, Columbia, South Carolina 29208, USA
(Received 8 December 2008; published 19 February 2009)

We demonstrate direct evidence that a single-crystal-like aragonite platelet is essentially assembled with aragonite nanoparticles. The aragonite nanoparticles are readily oriented and assembled into pseudo-single-crystal aragonite platelets via screw dislocation and amorphous aggregation, which are two dominant mediating mechanisms between nanoparticles during biomineralization. These findings will advance our understanding of nacre's biomineralization process and provide additional design guidelines for developing biomimetic materials.

DOI: 10.1103/PhysRevLett.102.075502

PACS numbers: 62.20.F-, 46.50.+a, 81.07.-b, 87.85.J-

Seashells have long been identified as natural armor materials with superior mechanical strength and toughness. The structure of seashells has evolved through millions of years to a level of optimization not currently achieved in engineered materials [1]. One of the best examples is nacre (mother of pearl) that is found in the shiny interior of many mollusk shells. Nacre is composed of approximately 95 vol.% brittle inorganic aragonite (a mineral form of CaCO_3) and a small percentage of organic biopolymer [2]. This material has a brick-and-mortar-like structure with highly organized polygonal aragonite platelets of a thickness ranging from 200 to 500 nm and an edge length of about $5 \mu\text{m}$ sandwiched with a 5–20 nm thick organic biopolymer interlayer, which assembles the aragonite platelets together [3]. Previous transmission electron microscopy (TEM) studies showed that the electron diffraction patterns of individual aragonite platelets have characteristics of single-crystal electron diffraction [4–6]. It has long been thought that aragonite platelets are brittle single crystals. However, recent atomic force microscopy (AFM) observation [3,7,8] revealed that individual aragonite platelets in fact consist of a large number of nanometer-sized particles with an average size of 32–44 nm and the aragonite platelets are not brittle but ductile. This distinctly contradicts the fact that individual aragonite platelets scatter as single crystals in TEM diffraction. A key question is raised, but not answered: how do nacre's aragonite platelets exhibit a dual nature with the characteristics of both monocrystal and polycrystals (nanoparticles) in such a contradictory manner? Here we report new mechanisms that nature uses to fabricate nacre's aragonite platelets at the nanoscale.

In this Letter, natural nacre materials from California red abalone (*Haliotis rufescens*) that belong to the class of gastropoda were studied. The shells were collected alive in Santa Barbara, CA. To minimize the detrimental effect of drying on the structure of shells, they were cleaned and air delivered in ice to the laboratory where the experiments were conducted. Nacre samples were cut from the nacre layer of the shells with a water-cooled, low-speed diamond

saw. Then the nacre samples were rinsed thoroughly with distilled water. The TEM samples were prepared by sectioning the nacre using the microtome technique (Micom HM 325 Rotary Paraffin Microtome) and then transferred onto the holey carbon-coated copper film for observation in a JEOL JEM 2100F transmission electron microscope with an accelerating voltage of 200 kV.

Nacre's cross section resembles a brick wall with aragonite platelets with [001] orientation toward organic biopolymer interlayers, as shown in Fig. 1(a). The electron diffraction patterns of individual aragonite platelets exhibit characteristics of a single crystal [Fig. 1(b)]. The high resolution TEM (HRTEM) image [Fig. 2(a)] reveals that individual aragonite platelets consist of a large number of nanoparticles. This is in good agreement with the recent AFM observation [3,7,8]. Fast Fourier transformation (FFT) analysis reveals that these nanoparticles are aragonite [see inset in Fig. 2(a)]. Some nanoparticles in the platelet hold the same crystal orientation. Here, let us take two particles in the boxed area in Fig. 2(a) as an example. Lattice fringe details [Fig. 2(b)] suggest that the interface between the two adjacent nanoparticles involves a slip of one particle relative to the other along [010]

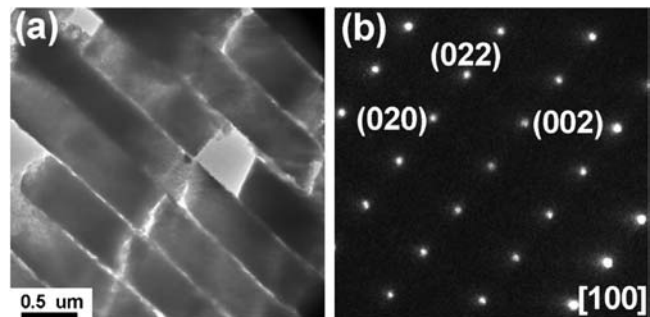


FIG. 1. Structural characterization of nacre. (a) TEM image of nacre's cross section, showing a brick wall-like architecture with aragonite platelets sandwiched with organic biopolymer interlayers. (b) Electron diffraction pattern of aragonite platelets, exhibiting single-crystal diffraction characteristics.

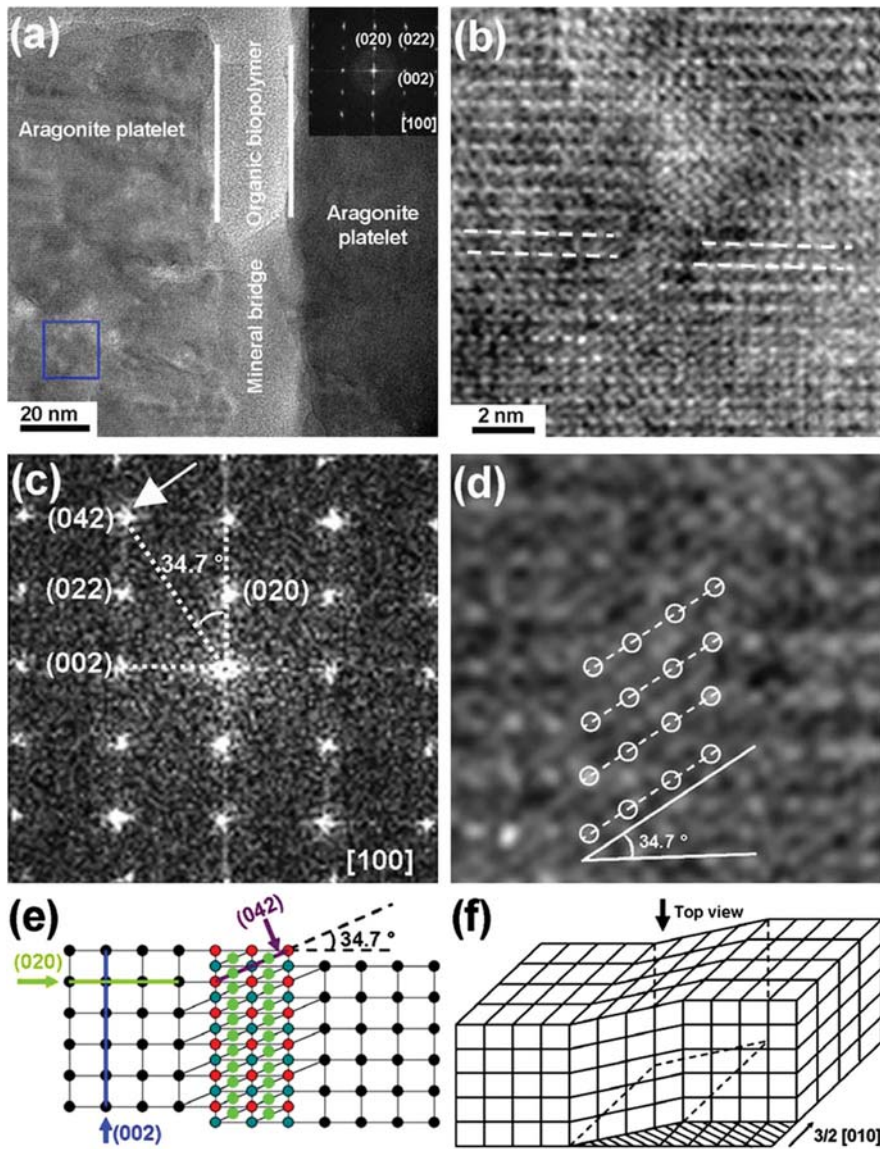


FIG. 2 (color). Observation and analysis of screw dislocation. (a) TEM image of two aragonite platelets with an organic biopolymer interlayer and a mineral bridge. (b) HRTEM image of the boxed area in Fig. 2(a), showing a screw dislocation lining two adjacent particles. (c) FFT pattern of the image in Fig. 2(b). (d) Close-up view of the atomic arrangement of the interface between the two adjacent nanoparticles. (e) Schematic showing that crystallographic planes linking the two adjacent nanoparticles are determined to be aragonite (042) planes. (f) Screw dislocation is visualized by considering slipping across the two adjacent nanoparticles by one and a half of lattice vector $\frac{3}{2}[010]$.

direction. Atomic arrangement at the interface is crystallographically different from that of the two adjacent particles, but the interface atoms are still packed in an ordered and repeated manner. The crystallographic planes linking the two adjacent nanoparticles were determined to be aragonite (042) planes [Figs. 2(b)–2(d)], which are schematically illustrated in Fig. 2(e). Such a type of crystallographic defect can be visualized as a screw dislocation, numerically corresponding to slipping across the two adjacent nanoparticles by one and a half of lattice vector $\frac{3}{2}[010]$. Figure 2(f) is a three-dimensional schematic illustration showing how the two adjacent aragonite nanoparticles are assembled via such screw dislocation in a parallel manner.

Why does nature assemble aragonite nanoparticles through such a screw dislocation mechanism? Indeed, several independent studies reported screw dislocation-based spiral growth of aragonite platelets [9–13]. However, the assembly mechanism of the aragonite nano-

particles inside individual platelets is completely unknown. The aragonite nanoparticles are defect-free crystals with unsatisfied surface bonds exposed to the mineral-solution or the mineral-organic interface during the biomineralization process. Thermodynamically, the assembly of aragonite nanoparticles is preferentially driven via reducing overall surface energy associated with the surface unsatisfied bonds. This requires that aragonite nanoparticles be oriented and attached to other nanoparticles or nanoparticle clusters. Such imperfect coherence between nanoparticles is realized in nacre by low energy driven screw dislocation. A similar assembly strategy was also demonstrated in a nanocrystalline titania particle system [14].

It was also found that in a single aragonite platelet, some nanoparticles do not hold the same crystal orientation, but why does the platelet exhibit single-crystal diffraction characteristics? Figure 3 shows the HRTEM images and corresponding FFT patterns of the nanoparticles in an

aragonite platelet. The FFT pattern [inset in Fig. 3(a)] from the whole image of Fig. 3(a) clearly exhibits single-crystal diffraction characteristics. Figure 3(a) contains at least three nanoparticles, as indicated by boxed areas b, c, and d in the figure. The FFT patterns of these three boxed areas reveal that particles b, c, and d have different crystal orientations. The diffraction patterns of particles b, c, and d can be indexed [100], $[1\bar{1}0]$, and $[2\bar{2}1]$ zones, respectively. When the three diffraction patterns are superposed [Figs. 3: (b'') + (c'') + (d'')], surprisingly, they form a single-crystal-like diffraction pattern [Fig. 3(a'')], i.e., pseudo-single-crystal effect. The unique crystal structure of aragonite and the arrangement of the aragonite nanoparticles in nacre's platelets make the diffraction patterns of individual platelets show single-crystal characteristics, which have confused us for decades.

Geometrically speaking, it is impossible that all aragonite nanoparticles are assembled by screw dislocation to achieve a high packing density. What is the other mechanism that works together with screw dislocation to assemble aragonite nanoparticles into individual platelets? We found amorphous phase between some aragonite nanoparticles, as shown in boxed area e in Fig. 3(a). This suggests that amorphous aggregation is another mediating mechanism between nacre's aragonite nanoparticles during the biomineralization process. The amorphous layer between nanoparticles would assist the particles' rotation and hold the surrounding nanoparticle clusters to share a specific crystallographic orientation. Figure 4 shows such an aragonite nanoparticle being assembled (docked) to the assembled aragonite platelet. It is believed that screw dislocation and organic biopolymer

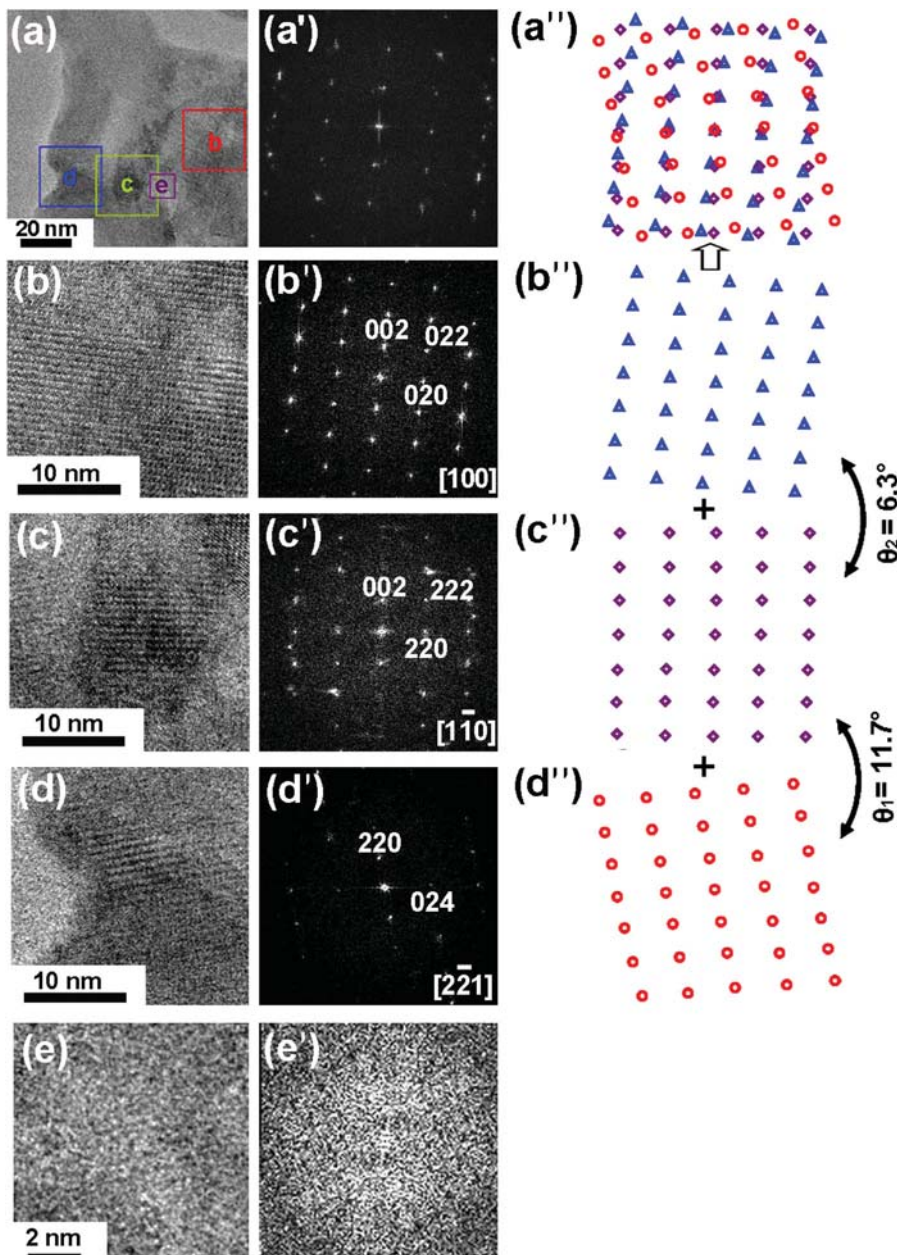


FIG. 3 (color). Pseudocrystal effect. (a) HRTEM image of an aragonite platelet. (b)–(e) Close-up views of boxed areas b, c, d, and e in (a). (a')–(e') Respective FFT patterns of (a)–(e). (a'')–(d'') Schematics of FFT patterns from corresponding images showing (b'') + (c'') + (d'') = (a'').

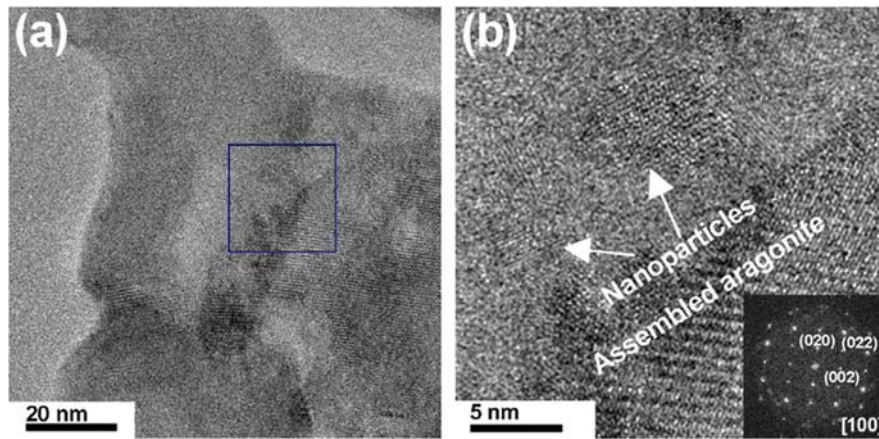


FIG. 4 (color). Nanoparticle assembly characteristics. (a) HRTEM image of an aragonite platelet. (b) Close-up view of two nanoparticles attached to the assembled aragonite platelet.

aggregation work together in assembling aragonite nanoparticle into individual platelets.

In summary, we have demonstrated direct evidence that a single-crystal-like aragonite platelet is essentially assembled with aragonite nanoparticles. Screw dislocation and amorphous aggregation are two dominant mediating mechanisms between nanoparticles during nacre's biomineralization process. The unique crystal structure of aragonite and the arrangement of the aragonite nanoparticles in nacre's platelets make the diffraction patterns of individual platelets exhibit single-crystal characteristics.

This work was supported by the U.S. Army Research Office under agreement/grant No. W911 NF-07-1-0449. We thank R. Z. Wang for providing the nacre samples.

*Corresponding author.

lixiao@engr.sc.edu

<http://www.me.sc.edu/research/nano/>

- [1] B. Mohanty, K. S. Katti, D. R. Katti, and D. Verma, *J. Mater. Res.* **21**, 2045 (2006).
 [2] A. P. Jackson, J. F. V. Vincent, and R. M. Turner, *Proc. R. Soc. B* **234**, 415 (1988).

- [3] X. D. Li, W. C. Chang, Y. J. Chao, R. Z. Wang, and M. Chang, *Nano Lett.* **4**, 613 (2004).
 [4] Q. L. Feng, F. Z. Cui, G. Pu, R. Z. Wang, and H. D. Li, *Mater. Sci. Eng., C* **11**, 19 (2000).
 [5] N. Nassif, N. Pinna, N. Gehrke, M. Antonietti, C. Jager, and H. Colfen, *Proc. Natl. Acad. Sci. U.S.A.* **102**, 12653 (2005).
 [6] F. Barthelat, C. M. Li, C. Comi, and H. D. Espinosa, *J. Mater. Res.* **21**, 1977 (2006).
 [7] M. Rousseau, E. Lopez, P. Stempfle, M. Brendle, L. Franked, A. Guetted, R. Naslain, and X. Bourrat, *Biomaterials* **26**, 6254 (2005).
 [8] X. D. Li, Z. H. Xu, and R. Z. Wang, *Nano Lett.* **6**, 2301 (2006).
 [9] K. Wada, *Nature (London)* **211**, 1427 (1966).
 [10] M. Fritz, A. M. Belcher, M. Radmacher, D. A. Walters, P. K. Hansma, G. D. Stucky, D. E. Morse, and S. Mann, *Nature (London)* **371**, 49 (1994).
 [11] S. Blank, M. Arnoldi, S. Khoshnavaz, L. Treccani, M. Kuntz, K. Mann, G. Grathwohl, and M. Fritz, *J. Microsc.* **212**, 280 (2003).
 [12] N. Yao, A. Epstein, and A. Akey, *J. Mater. Res.* **21**, 1939 (2006).
 [13] K. Tushtev, M. Murck, and G. Grathwohl, *Mater. Sci. Eng., C* (to be published).
 [14] R. L. Penn and J. F. Banfield, *Science* **281**, 969 (1998).



Nanoscale structural and mechanical characterization of heat treated nacre

Zaiwang Huang, Xiaodong Li*

Department of Mechanical Engineering, University of South Carolina, 300 Main Street, Columbia, SC 29208, USA

ARTICLE INFO

Article history:

Received 17 December 2008

Received in revised form 25 January 2009

Accepted 7 February 2009

Available online 23 February 2009

Keywords:

Nacre

Heat treatment

Structure

Mechanical property

Hardness

Elastic modulus

ABSTRACT

Nanoscale structural and mechanical characterization of heat treated nacre has been carried out. Two phase transformations were identified, i.e., from aragonite to calcite in the 500 °C heat treated nacre and from aragonite to calcium oxide (CaO) in the 1000 °C heat treated nacre. The brick-mortar architecture remains in the 500 °C heat treated nacre, but loses in the 1000 °C heat treated nacre. The heat treatment burned out the biopolymer in nacre. Nanoscale holes were discovered at the aragonite platelet boundaries and on the platelet surfaces. The heat treated nacre exhibits a sharp loss in elastic modulus and hardness compared with the fresh nacre.

© 2009 Elsevier B.V. All rights reserved.

1. Introduction

The structure of seashells has evolved through millions of years to a level of optimization, currently unreachable in engineered materials [1]. Nacre (mother-of-pearl), which is found in the shiny interior of many mollusk shells, is one of the most attractive natural biological materials with superior mechanical properties that have fascinated scientists and engineers over decades [2–4]. This material is composed of 95 vol.% inorganic aragonite (a mineral form of CaCO_3) and only a small percent of organic biopolymer. The most important structural characteristic of nacre is its brick-mortar architecture with highly organized polygonal aragonite platelets (bricks) of a thickness ranging from 200 to 500 nm and an edge length of about 5 μm , sandwiched with a 5–20 nm thick organic biopolymer interlayer (mortar), which glues the aragonite platelets together [4]. To date, the majority of research on nacre has been focused on how Mother Nature builds up such a unique ceramic/polymer hierarchical laminated composite from the bottom-up, and why nacre can achieve high strength without compensating its toughness. It has long been thought that nacre's aragonite platelets are brittle single crystals and nacre's ultrahigh strength and toughness mainly originate from crack deflection at the organic biopolymer interlayer, which dissipates more energy during the crack travel [5–7]. The organic matrix composed of proteins, such as Lustrin A, which has a highly modular structure, i.e., a multidomain architecture with folded modules, serves as an adhesive binding, the platelets together. In order to break the molecule chain with folded modules, a significant amount of energy is required to unfold each

individual module, which also contributes to the high toughness of nacre [8]. Recently mineral bridges were found between nacre's aragonite platelets, and are believed to act as 'ribs' to hold the aragonite platelets together, which contribute significantly to nacre's mechanical robustness [9]. Another important finding is the surface nanoasperities on nacre's aragonite platelets [10]. The surface nanoasperities were found to interlock neighboring platelets against sliding, which mainly renders nacre's inelasticity. Our recent studies on the nanostructure and nanomechanics of nacre using atomic force microscopy (AFM) and nanoindentation techniques have revealed that the individual aragonite platelets in fact consist of millions of nanosized particles (grains) with an average particle size of 32 nm and the aragonite platelets are not brittle, but ductile [3,4,11]. These nanoparticles can rotate and deform in the deformation of nacre. Rotation and deformation of aragonite nanoparticles are the two prominent mechanisms contributing to energy dissipation in nacre. The biopolymer spacing between nanoparticles facilitates the particle rotation process.

Nacre is a natural body armor material with superior mechanical properties. Can we extend the application of nacre to high temperature regime? At what temperature range can nacre remain its structural characteristics and mechanical robustness? On the other hand, nacre aragonite and biopolymer are natural biological materials and they may exhibit different phase transformation characteristics from the same types of man-made engineering/ synthetic materials. An in-depth understanding of phase transformation of nacre at high temperature helps improve the design of bioinspired materials that have better high temperature performance and can be used in harsh environments. To date, however, little is known about nacre's high-temperature structure and mechanical properties. How does thermal treatment affect nacre's multiscale architecture and mechanical

* Corresponding author.

E-mail address: lixiao@engr.sc.edu (X. Li).

URL: <http://www.me.sc.edu/research/nano> (X. Li).

robustness? Can we learn more from the heat treated nacre? In this study, the structure of both fresh and heat treated nacre samples was characterized using an X-ray diffractometer, an atomic force microscope (AFM), a scanning electron microscope (SEM), and a high resolution transmission electron microscope (HRTEM). The thermogravimetric behavior of nacre was studied using a thermogravimetric analyzer. The hardnesses and elastic moduli of both fresh and heat treated nacre samples were measured using a nanoindenter. Phase transformation mechanisms and the resulted mechanical properties are discussed in conjunction with brick-mortar architecture, nanoparticles inside nacre's platelets and biopolymer degradation during the heat treatment process. The findings reported here will advance our understanding of nacre's high temperature structure and mechanical properties and will provide application guidelines for nacre and its bioinspired materials.

2. Experimental

Natural nacre materials from California red abalone (*Haliotis rufescens*), which belong to the class of gastropoda, were studied. The shells were collected alive in Santa Barbara, CA. To minimize the detrimental effect of drying on the structure of the shells, they were cleaned and air delivered in ice to the laboratory where the experiments were conducted. Nacre samples were cut from the nacre layer of the shells with a water-cooled, low-speed diamond saw. They were then mechanically ground and polished using abrasives and powders down to 50 nm in size and rinsed thoroughly with distilled water prior to testing. The nacre samples were air heated for 10 min at 500 °C and 1000 °C, respectively, and subsequently air cooled down to room temperature.

The structure of both fresh nacre (without heat treatment) and heat treated nacre was characterized using a Rigaku D/Max-2100 powder X-ray diffractometer with Bragg–Brentano geometry and Cu K α radiation, a FEI Quanta 200 environmental SEM, a Veeco Dimension 3100 AFM system (Veeco Metrology Group), and a JEOL JEM 2100F HRTEM with an accelerating voltage of 200 kV. Thermogravimetric analysis (TGA) and differential thermal analysis (DTA) were performed on nacre using a Thermal Analysis Instruments SDT2960 Thermogravimetric Analyzer, and the sample was scanned at a rate of 20 °C per minute. Weight loss of the heat treated nacre samples was measured before and after heat treatment.

The hardnesses and elastic moduli of the nacre samples with and without heat treatment were measured using a Triboscope nanomechanical testing system (Hysitron Inc.) in conjunction with the Veeco system. The Hysitron nanoindenter monitored and recorded the load

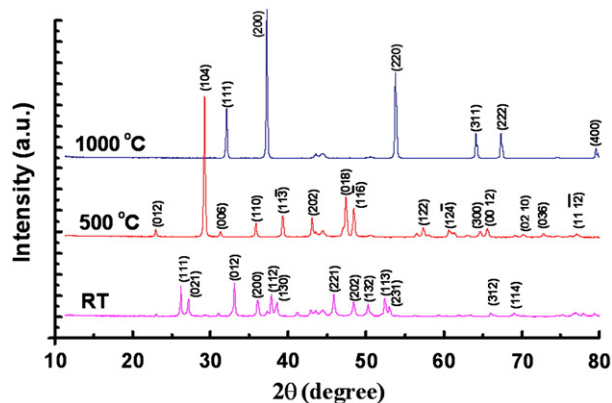


Fig. 2. XRD spectra of the nacre samples with and without heat treatment.

and displacement of the indenter, a diamond Berkovich three-sided pyramid, with a force resolution of about 50 nN and displacement resolution of about 0.1 nm. Hardness and elastic modulus were calculated from the recorded load-displacement curves. The indentation impressions were then imaged using the Veeco AFM.

3. Results and discussion

Fig. 1 shows the TGA and DTA curves of a fresh nacre sample heated up to 1000 °C in air. The weight loss was found to be about 3.6% between 264 °C and 451 °C with two major slope changes in the TGA curve, which is about the weight percentage of the biopolymer in the fresh nacre. The first stage is in the temperature range of 264–348 °C with a weight loss of 2.3%, which is attributed to the decomposition of the organic matrix [12]. The weight loss in the first stage is accompanied by an endothermic reaction at 278 °C in the DTA curve. The second stage proceeds between 348 °C and 451 °C with a weight loss of 1.3%, which results from the burning-out of the entire decomposition biopolymer matrix. The DTA curve also reveals that an endothermic transformation of aragonite to calcite occurred at 446 °C. Another weight loss of 41% occurred in the temperature range of 662–824 °C due to the phase transformation from calcite to calcium oxide (CaO), accounting for 44% of CO $_2$ (theoretical value) in the decomposition of calcite [12,13]. The corresponding endothermic effect was found at 808 °C in the DTA curve.

The XRD spectra of the nacre samples with and without heat treatment are shown in Fig. 2. All XRD peaks obtained from the fresh nacre can be well indexed as aragonite. Aragonite, packed by orthorhombic unit cells with lattice parameters $a = 4.962$ Å, $b = 7.968$ Å, and $c = 5.743$ Å, is well known as a metastable polymorph of calcium carbonate (CaCO $_3$). After a 10 min heat treatment at 500 °C, the aragonite transformed to calcite (a more stable polymorph of CaCO $_3$). In addition, the 500 °C heat treated sample exhibits a 3.7% weight loss, which is approximately the weight percentage of the biopolymer in the fresh nacre and the results are in good agreement with the TGA data (see Fig. 1). This indicates that 500 °C heat treatment burned out the biopolymer in nacre. The 10 min heat treatment at 1000 °C resulted in another phase transformation from calcite to calcium oxide (CaO), accompanied with a 45.3% weight loss which is also in consistency with the TGA result.

Fig. 3 shows the SEM images of the fresh and heat treated nacre samples. The fresh nacre exhibits the brick-mortar architecture with polygonal aragonite platelets assembled by the biopolymer “glue” (Fig. 3a). The biopolymer was found to serve as an adhesive to hold the aragonite platelets (Fig. 3b). Nanoscale asperities were found on the aragonite platelet surfaces, as shown in Fig. 3c. Compared with the fresh nacre, the 500 °C heat treated nacre keeps the brick-mortar architecture (Fig. 3d) although they have transformed from aragonite to calcite according to our DAT and XRD results in Figs. 1 and 2. Detailed SEM examination of the platelet surfaces reveals nanoscale

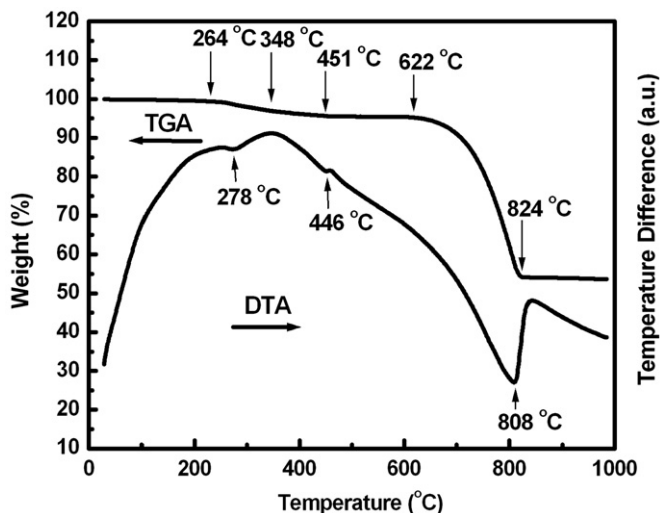


Fig. 1. TGA and DTA curves of a fresh nacre sample heated up to 1000 °C in air.

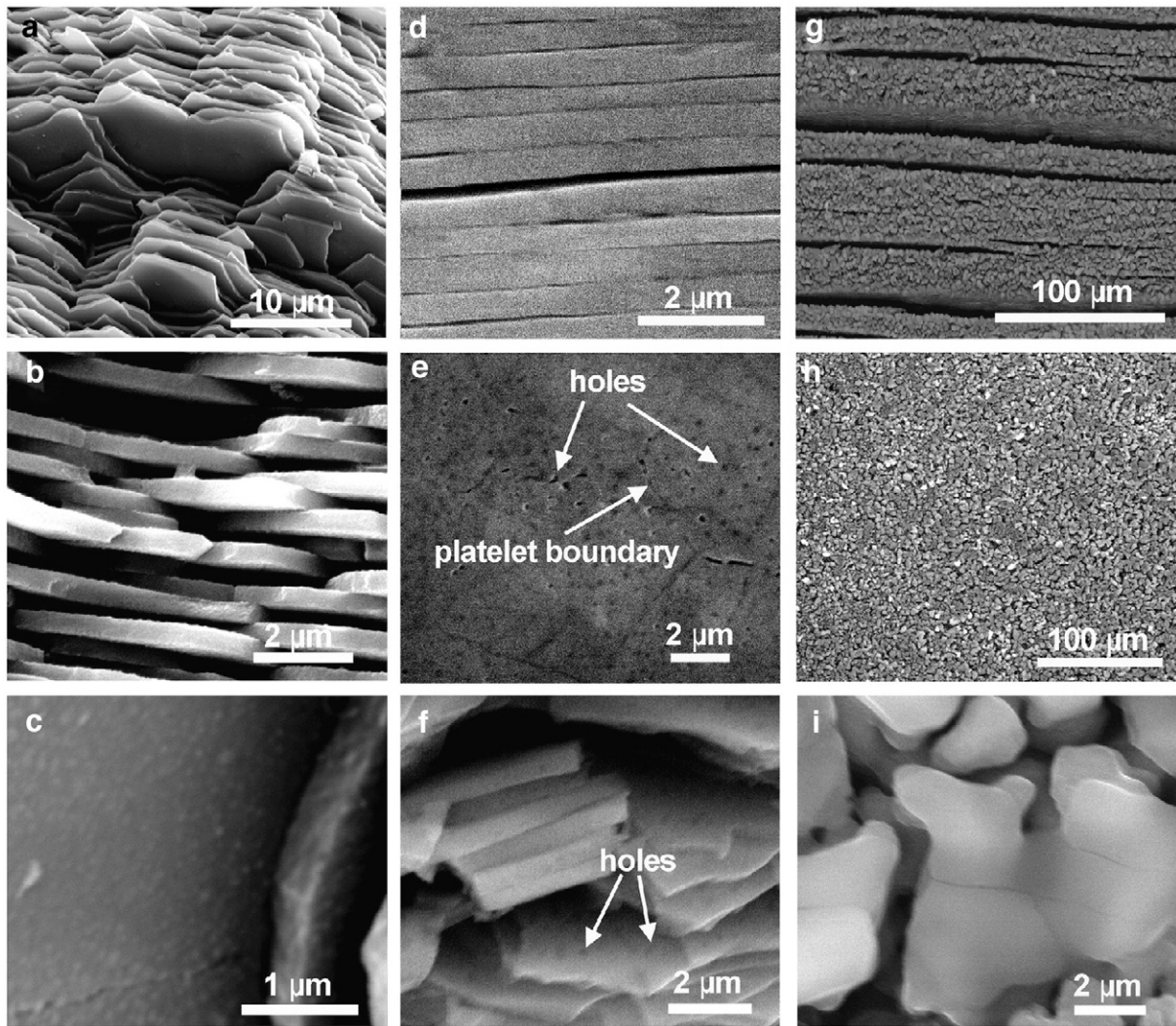


Fig. 3. SEM images of the fresh and heat treated nacre samples. (a) and (b) SEM images of the fracture surface of the fresh nacre sample, showing brick-mortar architecture and polygonal shape platelets (a) and the organic biopolymer is found to serve as adhesive to hold aragonite platelets (b). (c) SEM image of nanoasperities on the fresh nacre's aragonite surfaces. (d) SEM image of the cross section of the 500 °C heat treated nacre, showing brick-mortar laminated architecture and crack-like gaps between platelets. (e) SEM image of the platelet surfaces of the 500 °C heat treated nacre, showing nanoscale holes at the platelet boundaries and on the platelet surfaces. (f) SEM image of the fracture surface of the 500 °C heat treated nacre, showing nanoscale holes on the platelet surfaces. (g) SEM image of the cross section of the 1000 °C heat treated nacre, showing porous laminated architecture and crack-like gaps. (h) SEM image of the platelet surfaces of the 1000 °C heat treated nacre, showing porous structure without the platelet characteristic. (i) SEM image of the fracture surface of the 1000 °C heat treated nacre, showing microsized calcium particles.

holes at the platelet boundaries and on the platelets, as shown by arrows in Fig. 3e and f. The cross sectional SEM image shows that the biopolymer interlayers between platelets disappeared after the heat

treatment, leaving crack-like gaps on the cross section. Our previous studies [3,4,11] revealed that individual aragonite platelets are composed of millions of nanosized particles (grains) with an average

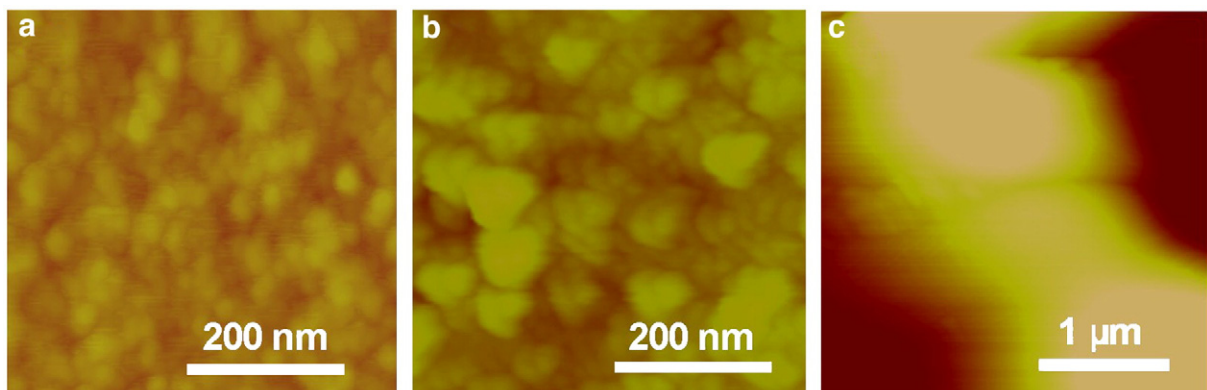


Fig. 4. AFM images of (a) the fresh nacre, (b) the 500 °C heat treated nacre, and (c) the 1000 °C heat treated nacre.

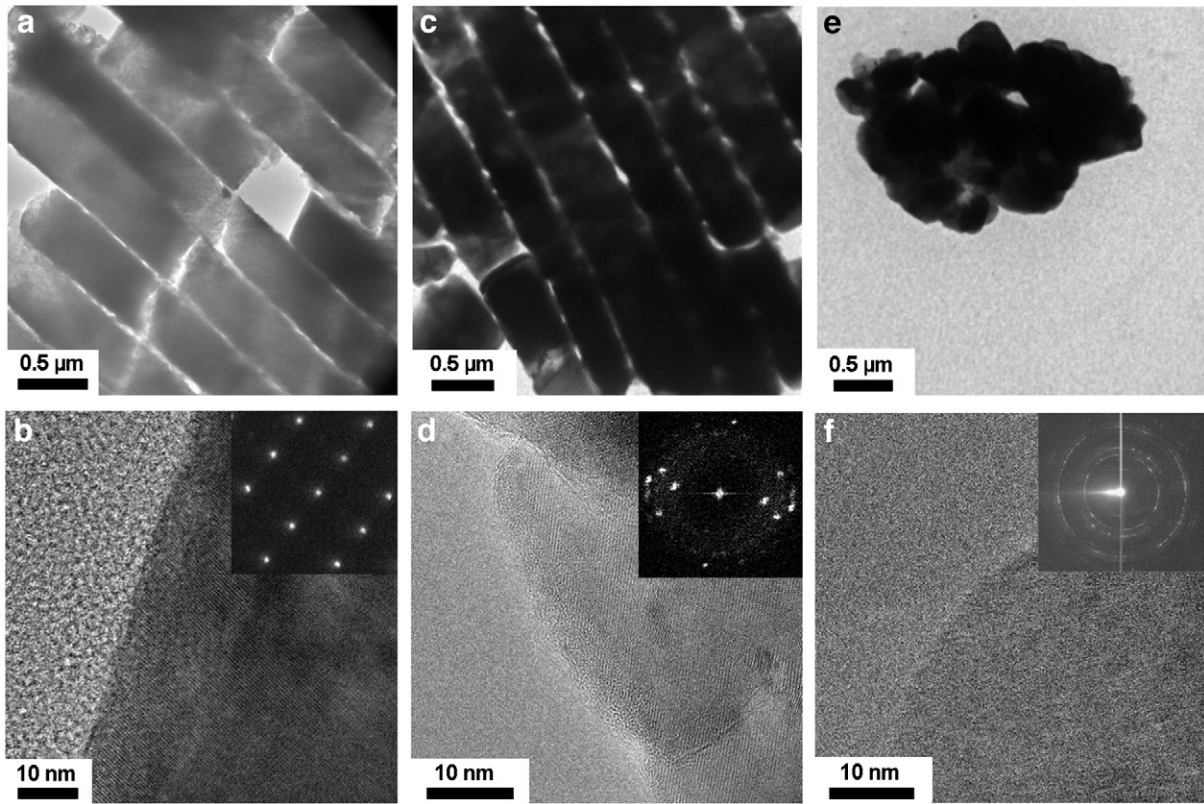


Fig. 5. TEM images of the (a, b) fresh nacre, (c, d) the 500 °C heat treated nacre, and (e, f) the 1000 °C heat treated nacre.

particle size of 32 nm. Between these nanoparticles exists a thin layer of biopolymer. It is believed that these holes on the platelet surfaces and crack-like gaps on the cross section of the heat treated nacre were previously filled with biopolymer, and burned out during the heat

treatment. The discovered nanoscale holes on the platelet surfaces in turn confirm our previous finding – existence of nanoparticles in individual aragonite platelets. The 1000 °C heat treated nacre still exhibits the characteristics of a laminated structure on the cross

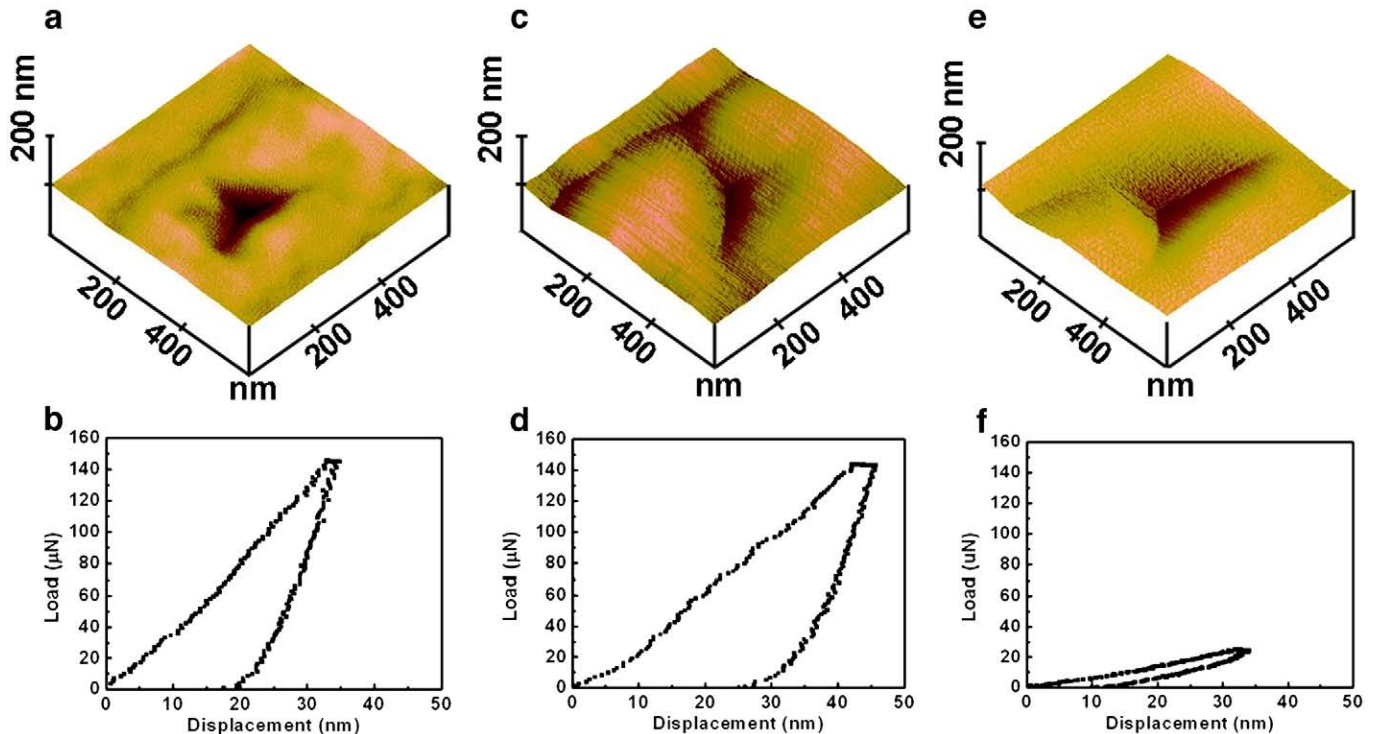


Fig. 6. AFM images of nanoindentation impressions and corresponding nanoindentation load-displacement curves for (a, b) the fresh nacre, (c, d) the 500 °C heat treated nacre, and (e, f) the 1000 °C heat treated nacre.

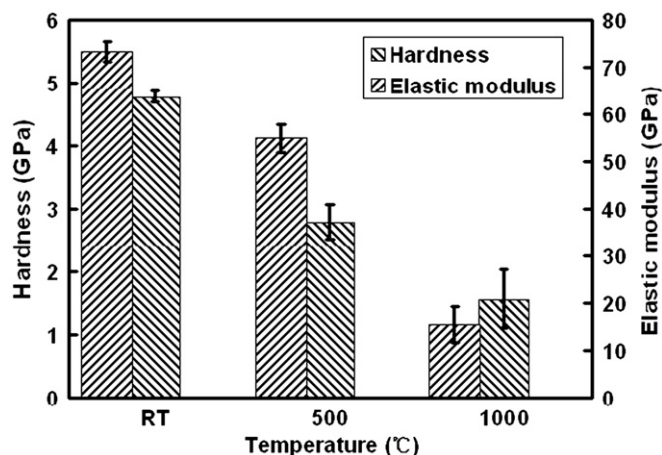


Fig. 7. Hardnesses and elastic moduli of the fresh and heat treated nacre.

section (Fig. 3g), but loses the polygonal feature on the top view (Fig. 3h). The high magnification SEM images (Fig. 3h and i) reveal microsized calcium oxide particles, which might result from the growth and/or aggregation of calcite nanoparticles during the heat treatment at 1000 °C.

AFM was also used to image the nanoscale morphologies of the nacre samples. The fresh nacre aragonite surface exhibits nanoparticle feature with an average particle size of 30–40 nm, as shown in Fig. 4a, in good agreement with our previous observation [3,4,11]. The nanoparticle feature survived, but grew up to an average particle size of 70–90 nm after the 500 °C heat treatment (Fig. 4b). This indicates that individual aragonite nanoparticles transformed into bigger calcite nanoparticles via individual particle growth and/or agglomeration. Further heat treatment at 1000 °C resulted in microsized calcium oxide particle formation, as shown in Fig. 4c.

The cross sectional HRTEM image (Fig. 5a) reveals that the fresh nacre has a brick-mortar structure with individual aragonite platelets sandwiched together by biopolymer layers with mineral bridges. The aragonite platelets exhibit single crystal diffraction characteristics. Preferential orientation (*c*-axis) of nacre growth was identified as [001] direction (Fig. 5b). The 500 °C heat treated nacre illustrates the same brick-mortar architecture (Fig. 5c). It is clear that the biopolymer layers between the platelets disappeared after the heat treatment process. The selected area diffraction pattern shows ring-like polycrystalline characteristics with calcite particles of different orientations (Fig. 5d). It appears that the 1000 °C heat treated nacre still exhibits some degrees of the laminated structure characteristic but shows a more particle-like coarse microstructure (Fig. 5e). The diffraction pattern exhibits a ring-like feature and can be indexed as calcium oxide (Fig. 5f).

Nanoindentations were made on the cross sections of the fresh and heat treated nacre samples to determine their hardnesses and elastic moduli. Fig. 6 shows the representative AFM images of nanoindentation marks and corresponding nanoindentation load-displacement curves. At about the same indentation load of 150 μ N, the fresh nacre

sample exhibits a shallower indentation mark (Fig. 6a) and a smaller indentation displacement (Fig. 6b) than the 500 °C heat treated nacre (Fig. 6c and d). In addition, more pop-in marks were found in the loading curve of the 500 °C heat treated nacre than in that of the fresh nacre. This suggests that the 500 °C heat treated nacre is more brittle than the fresh nacre. At an indentation load of 25 μ N, which is 6 times lower than the indentation load used on the fresh and the 500 °C heat treated nacre samples, the 1000 °C heat treated nacre already exhibits 32 nm indentation displacement for which the fresh nacre needs a 150 μ N load to achieve. Fig. 7 summarizes the hardnesses and elastic moduli of the fresh and heat treated nacre samples. It can be seen that the fresh nacre exhibits the highest hardness and elastic modulus, followed by the 500 °C heat treated nacre and the 1000 °C heat treated nacre. The sharp loss in hardness and elastic modulus results from the phase transformation and the loss of biopolymer integrating the particles and platelets.

4. Conclusions

Nacre is not stable and will transform from aragonite to calcite to calcium oxide upon heating. The 500 °C heat treated nacre keeps the brick-mortar architecture with calcite nanoparticles inside individual platelets. Nanoscale holes were discovered at the platelet boundaries and on the platelet surfaces. The 1000 °C heat treated nacre loses the brick-mortar architecture characteristic with microsized calcium particles of various crystal orientations. The heat treated nacre exhibits a sharp loss in hardness and elastic modulus compared with the fresh nacre, which results from the phase transformation and the loss of biopolymer integrating the particles and platelets.

Acknowledgments

Financial support for this study was provided by the U.S. Army Research Office under agreement/grant W911 NF-07-1-0449. The content of this information does not necessary reflect the position or policy of the Government and no official endorsement should be inferred.

References

- [1] B. Mohanty, K.S. Katti, D.R. Katti, D. Verma, *J. Mater. Res.* 21 (2006) 2045.
- [2] A.P. Jackson, J.F.V. Vincent, R.M. Turner, *Proc. R. Soc. Lond., B Biol. Sci.* 234 (1988) 415.
- [3] X.D. Li, *JOM* 59 (2007) 71.
- [4] X.D. Li, W.C. Chang, Y.J. Chao, R.Z. Wang, M. Chang, *Nano Lett.* 4 (2004) 613.
- [5] Q.L. Feng, F.Z. Cui, G. Pu, R.Z. Wang, H.D. Li, *Mater. Sci. Eng. C* 11 (2000) 19.
- [6] R. Menig, M.H. Meyers, M.A. Meyers, K.S. Vecchio, *Acta Mater.* 48 (2000) 2398.
- [7] B.J.F. Bruet, H.J. Qi, M.C. Boyce, R. Panas, K. Tai, L. Frick, C. Ortiz, *J. Mater. Res.* 20 (2005) 2400.
- [8] B.L. Smith, T.E. Schaffer, M. Viani, J.B. Thompson, N.A. Frederick, J. Kindt, A. Belcher, G.D. Stucky, D.E. Morse, P.K. Hansma, *Nature* 399 (1999) 761.
- [9] F. Song, A.K. Soh, Y.L. Bai, *Biomaterials* 24 (2003) 3623.
- [10] R.Z. Wang, Z. Suo, A.G. Evans, N. Yao, I.A. Askay, *J. Mater. Res.* 16 (2001) 2485.
- [11] X.D. Li, Z.H. Xu, R.Z. Wang, *Nano Lett.* 6 (2006) 2301.
- [12] R. Knitter, C. Odemer, J. Hausselt, CFI, *Chemic. Forum Int.* 85 (2008) E38.
- [13] S. Yoshioka, Y. Kitano, *Geochem. J.* 19 (1985) 245.

Deformation Strengthening of Biopolymer in Nacre

Zhi-Hui Xu and Xiaodong Li*

Department of Mechanical Engineering, University of South Carolina, 300 Main Street,
Columbia, SC 29208, USA

* To whom correspondence should be addressed. E-mail: lixiao@cec.sc.edu

Abstract

Nacre is an ultra-tough natural nanocomposite found in mollusk shell consisting of hard aragonite nanocrystals and soft biopolymer matrix. Other than maintaining the integrity of nacre's brick-and-mortar nanoarchitecture, the biopolymer plays a critical role in the strengthening and toughening of nacre. By directly probing the biopolymer strands using an atomic force microscope, we unveiled that the biopolymer in nacre has the capability to strengthen itself during deformation. This unusual deformation strengthening mechanism contributes remarkably to the ultra-high toughness of nacre, which can be explained by a coil spring model. The findings advance the understanding of the mystery of nacre's toughening mechanisms, provide additional design guidelines for developing biomimetic nanomaterials, and lay a constitutive foundation for modeling the deformation behavior of nacre.

Keywords: Nacre; Biopolymer; Strengthening; Toughening; Atomic Force Microscopy.

1. Introduction

Nacre, also known as mother of pearl, is a natural nanocomposite material that forms the inner layer of many mollusk shells ^[1,2]. Consisting of about 95 wt. % brittle inorganic aragonite (a mineral form of CaCO_3) and 5% of organic biopolymer, nacre has a unique brick-and-mortar-like architecture with highly organized polygonal aragonite platelets of a thickness around 500 nm and an edge length about 5 μm embedded in the biopolymer matrix ^[3,4]. The combination of soft biopolymer and hard aragonite makes nacre 2-fold stronger and 1000-fold tougher than its constituent materials ^[1]. Such remarkable properties have motivated many researchers to reproduce nature's achievement by synthesizing biomimetic nanocomposites ^[5-8] and to understand the deformation and toughening mechanisms of nacre ^[9-24].

Previous studies have revealed that the toughening of nacre originates from its unique lamellar structure formed through millions of years of evolution. Several toughening mechanisms have been proposed based on experimental observation and computational modeling of the deformation and failure of nacre. On one hand, the ultra-high toughness of nacre has been related to the unique microstructural features of the aragonite platelets. For example, Evans *et al.* ^[11] and Wang *et al.* ^[12] attributed the ductility and toughening of nacre to the interaction of the surface nanoasperities on the aragonite platelets and the formation of dilatation bands. Song *et al.* ^[16] showed that the small mineral bridges between aragonite platelets play a key role in the mechanical robustness of nacre. Li *et al.* ^[17] found that aragonite nanoparticle rotation and deformation are the prominent mechanisms contributing to the inelasticity and toughening of nacre. Katti *et al.* ^[18] showed through finite element modeling that the interlocks between aragonite platelets play an important role in the strengthening and toughening of nacre. Barthelat *et al.* ^[19] argued that the surface waviness of the aragonite platelets could generate strain

hardening, spread the inelastic deformation, suppress damage localization leading to material instability, and thus contribute to the toughness of nacre. On the other hand, research has also been focused on the role of biopolymer matrix in the toughening of nacre. Smith *et al.* [20] found that the biopolymer molecule(s) in nacre matrix with a modular structure can unfold its modular domains during atomic force microscopy (AFM) extension and dissipates more energy compared to short molecule without modular, which contributes to both high tensile strength and high toughness of nacre. Evans *et al.* [11] hypothesized that the organic matrix enhances the toughness of nacre by creating a viscoelastic glue layer at the interface between adjacent platelets. Tushtev *et al.* [21] showed through finite element calculations that the thin layer of biopolymer plays a key role in the stress distribution in nacre and the high stiffness determined experimentally is only feasible if the organic layer is incompressible (Poisson's ratio equals 0.5). Meyers *et al.* [22, 23] investigated the biopolymer membrane on the growth surfaces of nacre and found that the organic layer exhibits significant strength and stiffness when it is dry but shows low modulus and strength and great extensibility in a fully hydrated state. Although much effort has been devoted to understanding the toughening mechanisms of nacre, it is still unknown what roles the biopolymer plays in the strengthening and toughening of nacre and how the biopolymer behaves during mechanical deformation.

2. Results and discussion

Fig. 1a shows a biopolymer strand with a length of 100 nm and a diameter about 36 nm that was stretched between two aragonite platelets. To probe the deformation behavior of the biopolymer strand, a RESEP tapping AFM probe was used to perform a bending test at the middle of the biopolymer strand as schematically shown in Fig. 1b. The probe has a sharp silicon tip with a nominal radius less than 10 nm for tapping AFM and a rectangle shape cantilever with

a spring constant $k = 34.4 \text{ N/m}$ ^[25]. During bending test, the cantilever approached to the biopolymer strand at a velocity of 144 nm/s (loading). When the tip was in contact with the biopolymer strand, the cantilever started to deflect up and a bending force was applied to the biopolymer strand. Once the cantilever deflection reached a preset threshold, the cantilever withdrew with the same velocity (unloading). The bending force was calculated using Hooke's law. A typical bending force-deflection curve of the biopolymer strand is shown in Fig. 1c. The loading curve normally consists of two linear segments with different slopes. The first segment is rather smooth reflecting an elastic deformation behavior of the biopolymer strand while the second segment shows random serrated features denoting inelastic behavior. The slope of the first segment is about 21.1 nN/nm while that of the second one is 94.9 nN/nm, which clearly indicates an increasing stiffness of the biopolymer strand with the increase of deformation. This kind of deformation strengthening of the matrix biopolymer will enhance both the strength and toughness of nacre. In fact, Marszalek *et al.* ^[26] also predicted a similar bilinear behavior in mechanically unfolding the modular protein titin using steered molecular dynamics simulations. The unloading curve does not overlap with the loading one, indicating inelastic deformation of the biopolymer strand and energy dissipation during the bending test.

Fig. 2a shows an AFM height image of three biopolymer strands stretched between two aragonite platelets. Two bending tests were performed consecutively on the right biopolymer strand highlighted with an arrow. Test 1(T1) consists of two bending experiments with the respective maximum forces of 144.6 nN and 342.2 nN. Test 2 (T2) consists of three bending experiments with the respective maximum forces of 148.2 nN, 350.9 nN, and 534.8 nN. Figs. 2b and 2c show the AFM height images of the right biopolymer strand after T1 and T2, respectively. As can be seen, the surface morphology of the biopolymer strand (highlighted with

the arrow) bended by AFM tip change dramatically after both tests while the other two biopolymer strands without any bending remain the same. Figs. 2d-f present the detailed surface profiles of the right biopolymer strand before bending (Fig. 2d), after T1 (Fig. 2e), and after T2 (Fig. 2f), respectively and the locations where the surface profiles were taken from. Clearly, the surface profiles of the biopolymer strand after T1 and T2 (Figs. 2e-f) become more bulging and rougher compared to that before bending (Fig. 2d). Fig. 2g shows two bending force-deflection curves from T1 and T2 with similar maximum bending forces of 144.6 nN (T1) and 148.2 nN (T2). It should be noted that T1 is performed on the biopolymer strand in a state shown in Fig. 2a while T2 on the same biopolymer strand in a state shown in Fig. 2b. The two bending force-deflection curves from T1 and T2 overlap each other very well at the initial bending. This also suggests that the initial deformation was mostly elastic. With the cantilever moving further down, the curves from T1 and T2 start to deviate from each other. At the same cantilever position, bending force for T1 is larger than that for T2, indicating a decrease in the stiffness of the biopolymer strand. Fig. 2h is a close-up of the loading curves of T1 and T2, which has a random serrated characteristic as highlighted by the arrows.

As discussed above, the bending process of a biopolymer strand of nacre matrix may be divided into three stages schematically shown in Fig. 3a. At the initial loading (stage 1), deformation of the biopolymer strand is mainly elastic with a relatively low stiffness (small slope of the bending force-deflection curve). With further increasing loading, deformation of the biopolymer strand becomes inelastic (stage 2) with high stiffness (large slope of the bending force-deflection curve). The unloading curve (stage 3) does not overlap with the loading one due to the inelastic deformation and the dark area between the loading and unloading curves is the dissipated energy through heat. The stiffness increase with deformation for the biopolymer

strand during loading reveals a new deformation toughening mechanism, which may be understood by considering the extension of single biopolymer molecule as a series of helical spring. It is well known that the biopolymer of nacre has highly modular structure that unfolds upon loading and refolds when unloading. Fig. 3b is a schematic of three modules of a single biopolymer molecule. Each module may be considered as a helical spring. The spring constant of the helical spring may be calculated by the following equation ^[27].

$$k_s = \frac{E d^4}{16n(1+\nu)(D-d)^3} \quad (1)$$

where k_s is the spring constant of biopolymer module, E and ν are the elastic modulus and Poisson's ratio of the biopolymer wire, respectively, d is the diameter of the biopolymer wire, n is number of active windings, and D is the spring outer diameter. When a small external load is applied to extend the biopolymer molecule, the deformation is elastic and mostly accommodated by stretching the bonds between the tangled biopolymer wires in the module. At certain critical load, the bonds between the tangled biopolymer wires start to break, leading to the unfolding of the biopolymer module. The biopolymer module may totally unfold as a straight wire as shown in Fig. 3c. The spring constant of the straight biopolymer wire k_w is given by

$$k_w = \frac{E d^2}{4n(D-d)} \quad (2)$$

Combine Equations 1 and 2, we have

$$\frac{k_s}{k_w} = \frac{1}{4(1+\nu)\left(\frac{D}{d}-1\right)^2} \quad (3)$$

From the geometry point of view, D must be larger than or at least equals to $2d$. This means the spring constant of the straight wire k_w is always larger than that of the biopolymer module. Therefore, the spring constant or stiffness of the biopolymer molecule increases with the unfolding of each module. This may explain the deformation strengthening of the nacre's biopolymer strand with high modular structure observed in this study. After releasing the external load, the unfolded biopolymer module will refold^[20, 28] as schematically shown in Fig. 3d. Since energy dissipation occurs during the unfolding and refolding of the biopolymer module, thermodynamically it is impossible to have the unfolded biopolymer wire refold to its original state as shown in Fig. 3b. Instead, the biopolymer wire will refold to form a rather loose module, which results in a more bulging and rougher biopolymer strand as observed in Figs. 2a-f. The difference in bending force-deflection curves observed in Figs. 2g-h may also be explained by the spring model considering the structure change in the biopolymer module as shown in Figs. 3b and 3d. When the bending force is small, the deformation is elastic and mainly accommodated by the extension of the bonding among the overlapped parts of the biopolymer wire. Since the chemical bonds among the overlapped parts of the biopolymer wire remain the same after refolding, the initial elastic parts of the bending force-deflection curves of T1 and T2 in Fig. 2g overlap each other very well. However, with further increase of the bending force, the chemical bonds start to break and biopolymer module starts to unfold and behave like a spring. As shown in Equation 1, the spring constant is inverse proportional to D^3 and thus the refolded biopolymer module with a larger D should have a spring constant k_s' smaller than k_s . This makes the refolded biopolymer strand behave more compliant than its original state leading to a stiffness decrease in T2 as shown in Fig. 2g. The serrated features of the bending force-

deflection curves shown in Fig. 2h may be due to the unfolding of the biopolymer module and/or the detaching of the biopolymer molecule from the aragonite platelets.

3. Conclusions

Bending test has been performed to probe the deformation behavior of the biopolymer strands of nacre's matrix using AFM. It is found that the biopolymer matrix in nacre has the capability to strengthen itself during deformation. A spring model has been proposed to explain the deformation strengthening mechanism. It is believed that the deformation strengthening mechanism of biopolymer matrix contributes to the ultra-high toughness of nacre together with other toughening mechanisms such as, crack deflection, deformability of aragonite platelets, aragonite platelet slip, interlocks from platelet surface nanoasperities, and rotation and deformation of nanoparticles. This finding may provide further understanding of the mystery of nacre's toughening, additional design guidelines for developing biomimetic nanomaterials, and a constitutive foundation for modeling of the deformation behavior of nacre.

4. Experimental

The nacre materials used in this study are from California red abalone (*Haliotis rufescens*) that belongs to the class of gastropoda. The shells were collected alive in Santa Barbara, CA. To minimize the detrimental effect of drying on the structure of shells, they were cleaned and air delivered in ice to the laboratory where the experiments were conducted. A notched beam specimen with dimension of 15 x 2.3 x 1.7 mm (length x height x width) was cut from the nacre layer of the shells with a water-cooled, low-speed diamond saw and the top surface of the specimen was mechanically ground and polished using abrasives and powders down to 50 nm in size (Fig. 4a). The specimen was then mounted to a custom-designed

micromechanical tester which was integrated with an AFM (Veeco Dimension 3100, Veeco Metrology Group, Santa Barbara, CA) to perform three-point bending test while AFM imaging was carried out simultaneously around the notch tip, where stress concentration occurred and nacre material was mainly subjected to tensile stresses. Upon tension, the nacre material around the notch tip was deformed and elongated and the biopolymer matrix between aragonite platelets was stretched to form the biopolymer strands as shown in Figs. 4b and 4c. Bending test was performed at the middle of the biopolymer strand using a RESEP tapping AFM probe to probe the deformation behavior of the biopolymer. The fractured nacre specimens were observed using a field emission scanning electron microscope (FE-SEM, Ultra Plus, Carl Zeiss SMT Inc., Peabody, MA) with an accelerating voltage of 5 kV. The SEM images (Figs. 4d and 4f) also show the biopolymer strands between the aragonite platelets.

Acknowledgments

This work was supported by the U.S. Army Research Office under agreement/grant No. W911 NF-07-1-0449. We thank Dr. R. Z. Wang for providing the nacre samples.

References

- [1] A.P. Jackson, J.F. Vincent, R.M. Turner, Proc R Soc London Ser B **1988**, 234, 415.
- [2] J.D. Curry, Proc R Soc London Ser B **1997**, 196, 443.
- [3] X.D. Li, W.C. Chang, Y.J. Chao, R.Z. Wang, M. Chang, Nano Lett **2004**, 4, 613.
- [4] M. Rousseau, E. Lopez, P. Stempfle, M. Brendle, L. Franke, A. Guette, R. Naslain, X. Bourrat, Biomater **2005**, 26, 6254.
- [5] Wang XX, Xie L, Wang R. Biological fabrication of nacreous coating on titanium dental implant. Biomaterials 2005;26:6229-32.
- [6] A. Sellinger, P.M. Weiss, A. Nguyen, Y. Lu, R.A. Assink, W. Gong, C.J. Brinker, Nature **1998**, 394, 252.
- [7] Z.Y. Tang, N.A. Kotov, S. Magonov, B. Ozturk, Nature Mater **2003**, 2, 413.
- [8] C. Ortiz, M.C. Boyce, Science **2008**, 319, 1053.
- [9] X.D. Li, P. Nardi, Nanotechnol **2004**, 15, 211.
- [10] S. Kamat, X. Su, R. Ballarini, A.H. Heuer, Nature **2000**, 405, 1036.
- [11] A.G. Evans, Z. Suo, R.Z. Wang, I.A. Aksay, M.Y. He, J.W. Hutchinson, J Mater Res **2001**, 16, 2475.
- [12] R.Z. Wang, Z. Suo, A.G. Evans, N. Yao, I.A. Aksay, J Mater .Res **2001**, 16, 2485.
- [13] X.D. Li, JOM **2007**, 59, 71.

- [14] B.J.F. Bruet, H.J. Qi, M.C. Boyce, R. Panas, K. Tai, L. Frick, C. Ortiz, *J Mater Res* **2005**, 20, 2400.
- [15] H.J. Gao, B.H. Ji, I.L. Jager, E. Arzt, P. Pratzl, *Proc Natl Acad Sci USA* **2003**, 100, 5597.
- [16] F. Song, A.K. Soh, Y.L. Bai, *Biomater* **2003**, 24, 3623.
- [17] X.D. Li, Z.H. Xu, R.Z. Wang, *Nano Lett* **2006**, 6, 2301.
- [18] K.S. Katti, D.R. Katti, S.M. Pradhan, A. Bhosle, *J Mater Res* **2006**, 21, 1237.
- [19] F. Barthelat, H. Tang, P.D. Zavattieri, C.M. Li, H.D. Espinosa, *J Mech Phys Solids* **2007**, 55, 306.
- [20] B.L. Smith, T.E. Schaffer, M. Viani, J.B. Thompson, N.A. Frederick, J. Kindt, A. Belcher, G.D. Stucky, D.E. Morse, P.K. Hansma, *Nature* **1999**, 399, 761.
- [21] K. Tushtev, M. Murck, G. Grathwohl, *Mater Sci Eng C* **2008**, 28, 1164.
- [22] M.A. Meyers, C.T. Lim, A. Li, B.R. Hairul Nizam, E.P.S. Tan, Y. Seki, J. McKittrick, *Mater Sci Eng C* **2009**, 29, 2398.
- [23] M.A. Meyers, A.Y.M. Lin, P.Y. Chen, J. Muiyco, *J Mech Behav Biomed Mater* **2008**, 1, 76.
- [24] H. Moshe-Drezner, D. Shilo, A. Dorogoy, E. Zolotoyabko, *Adv Funct Mater* 2010, 20, 2723.
- [25] Z.H. Xu, M.A. Sutton, X.D. Li, *Acta Mater*, **2008**, 56, 6304.
- [26] PE Marszalek, H Lu, H Li, M Carrion-Vazquez, AF Oberhauser, K Schulten, JM Fernandez. *Nature* **1999**, 402, 100.

[27] A.M. Wahl, Mechanical Springs, 1st ed., Penton Publishing Co., Cleveland, Ohio, **1944**.

[28] M. Kim, K. Abdi, G. Lee, M. Rabbi, W. Lee, M. Yang, C.J. Schofield, V. Bennett, P.E. Marszalek, Biophys J **2010**, 98, 3086.

Figure captions

Fig. 1. AFM bending of biopolymer strand. (a) AFM image of a single biopolymer strand stretched between aragonite platelets. (b) Schematic of the setup of AFM bending test. (c) A typical bending force-deflection curve of a biopolymer strand.

Fig. 2. Morphology changes and bending force-deflection curves of a biopolymer strand after a series of bending tests. (a) Original morphology of biopolymer strands. (b) Morphology of biopolymer strands after T1. (c) Morphology of biopolymer strands after T2. (d) – (f) surface profiles of the tested biopolymer strands of (a) – (c) respectively. (g) Bending force-deflection curves of T1 and T2. (h) Close-up of loading segments of curves in (g) showing the serrated features.

Fig. 3. Schematic of deformation strengthening mechanism of the biopolymer of nacre. (a) Bending force–deflection curve showing the three stages of deformation and the biopolymer strand before and after bending. (b) Biopolymer molecule with modular structure before extension. (c) Biopolymer molecule under extension with an unfolded module. (d) Biopolymer molecule after extension with a refolded module.

Fig. 4. Biopolymer strands stretched between aragonite platelets. (a) Schematic of a notched nacre beam. (b) AFM image of biopolymer strands stretched between aragonite platelets. (c) Close-up of biopolymer strands in (b). (d) FESEM image of biopolymer strands stretched between aragonite platelets. (e) Close-up of biopolymer strands in (d).

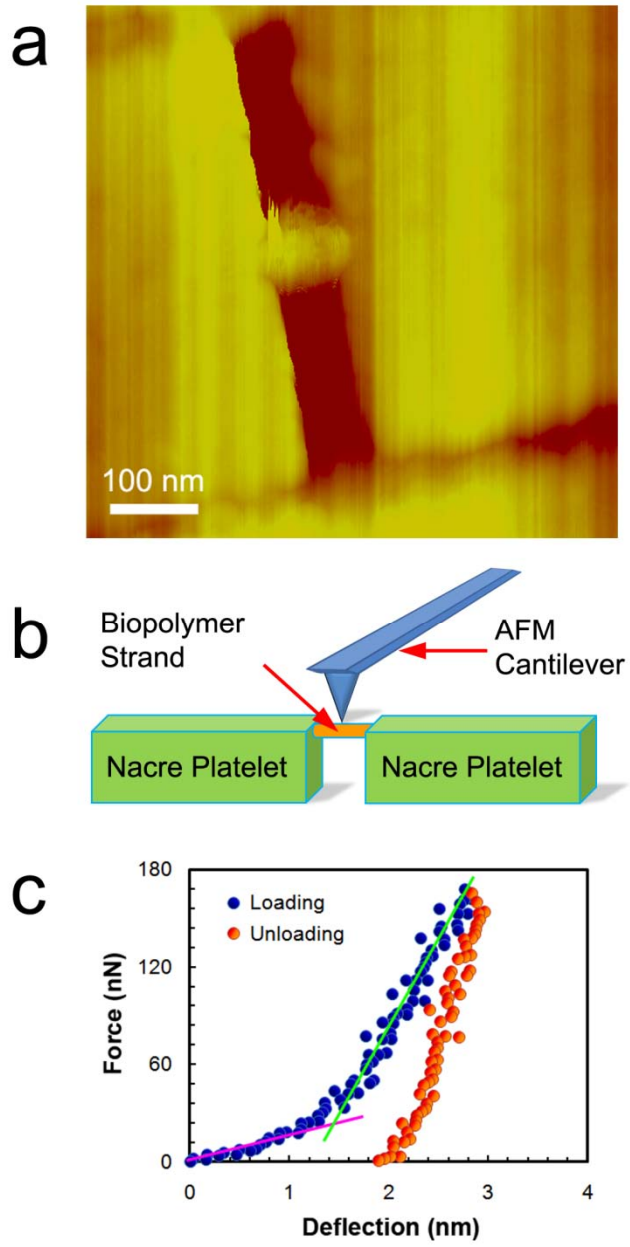


Figure 1

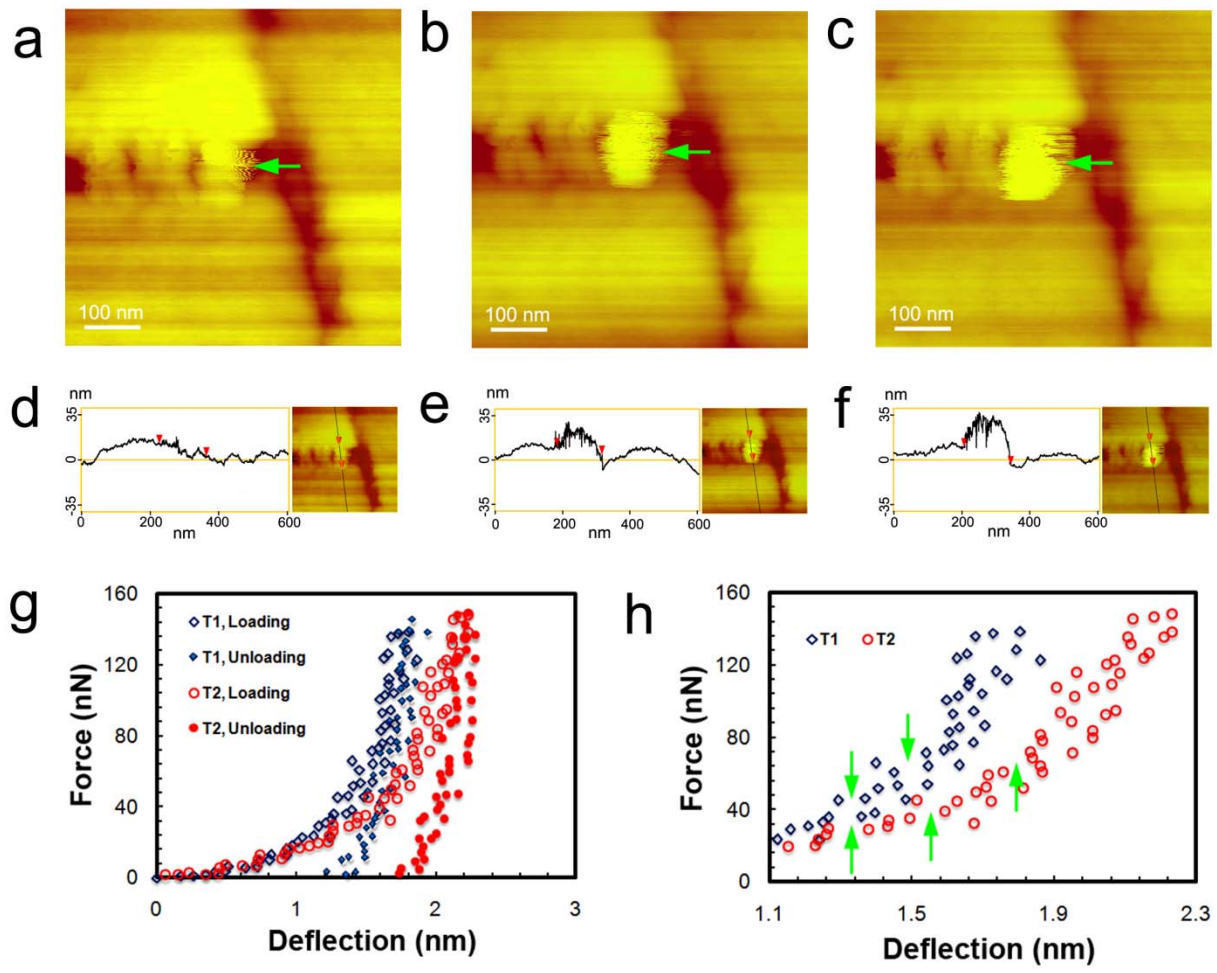


Figure 2

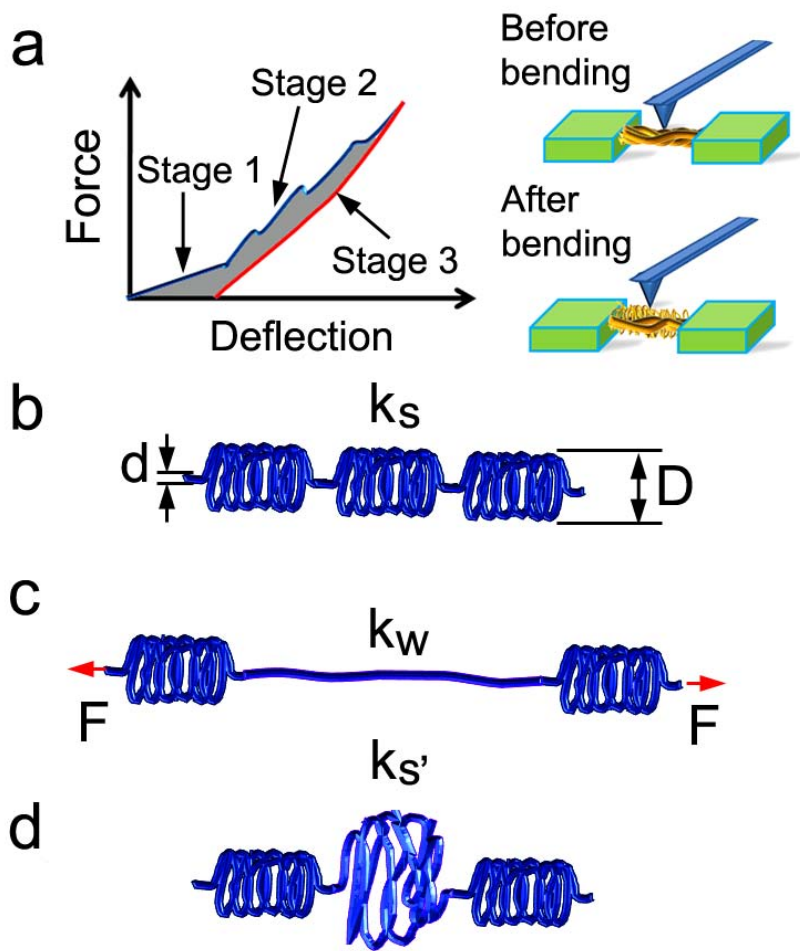


Figure 3

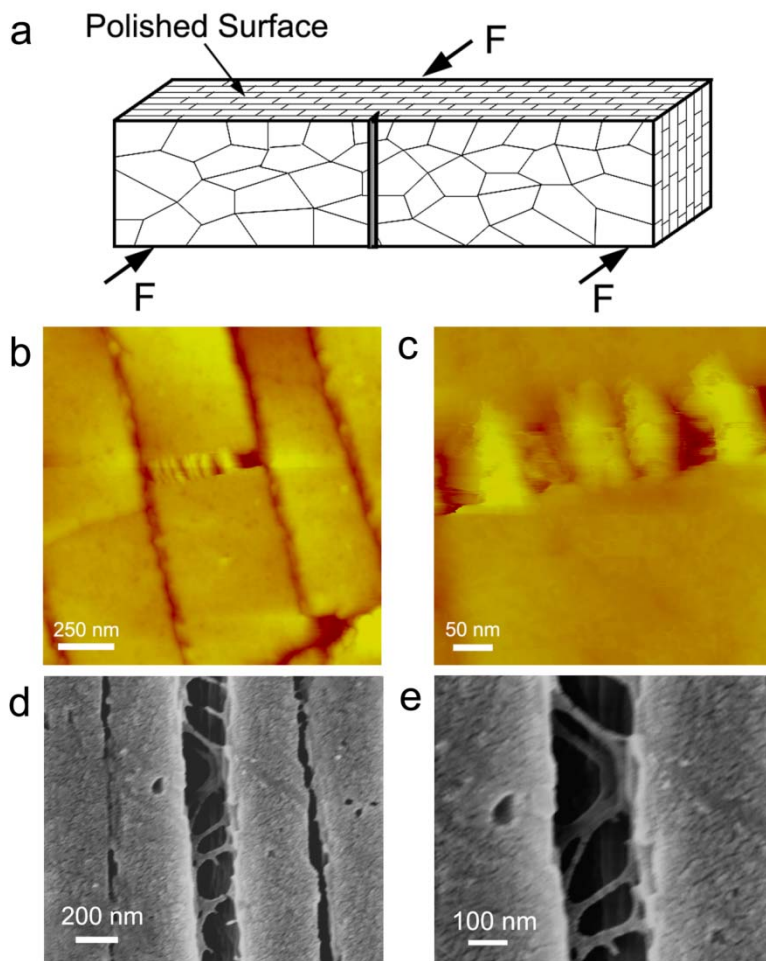


Figure 4

**Elastic modulus of biopolymer matrix in nacre measured using coupled atomic force
microscopy bending and inverse finite element techniques**

Zhi-Hui Xu, Yingchao Yang, Zaiwang Huang, Xiaodong Li*

Department of Mechanical Engineering, University of South Carolina, 300 Main Street,
Columbia, South Carolina 29208

* Corresponding author: lixiao@cec.sc.edu

Abstract

A novel approach combining atomic force microscopy probing of nacre biopolymer strand and inverse finite element analysis has been used to directly measure the elastic modulus of nacre biopolymer matrix. An elastic modulus of 10.57 ± 2.56 GPa was determined for nacre biopolymer matrix for the first time from the direct measurement. This property is essential for a fundamental understanding of the roles that the biopolymer matrix plays in nacre's strengthening and toughening, and provides guidelines in selecting engineering polymers for biomimetic materials design and fabrication. Such coupled experimental and modeling techniques should find more applications in studying the mechanical behavior of biological materials.

Keywords:

Elastic modulus; Biopolymer; Nacre; Atomic force microscopy; Inverse finite element.

1. Introduction

Nacre, also known as mother of pearl, is a natural material that forms the inner layer of many mollusk shells [1,2]. It consists of about 95% brittle inorganic aragonite (a mineral form of CaCO_3) and 5% of organic biopolymer arranged in a unique brick-and-mortar-like architecture, where highly organized polygonal aragonite platelets of a thickness around 500 nm and an edge length about 5 μm are embedded in a biopolymer matrix with a thickness of 5-20 nm [3]. Such laminated structure makes nacre 2 times stronger and 1000 times tougher than its constituent materials [1]. This has motivated many researchers to study the deformation and toughening mechanisms of nacre [4-13] and to reproduce nature's achievement by synthesizing biomimetic nanocomposites [14-16].

Several mechanisms have been reported contributing to the strengthening and toughening of nacre. This includes the interlocks between aragonite platelets due to nanoasperities on platelet surface [5,6] and penetration of adjacent platelets [7], strain hardening due to microscale waviness of the platelets [8], mineral bridge connection between aragonite platelets [9], and rotation and deformation of aragonite nanoparticles [10]. In addition to the significant contribution of aragonite platelets to the strengthening and toughening of nacre, the biopolymer matrix, although it just occupies 5% of the nacre structure, also plays extremely important role. The biopolymer layer not only regulates the nucleation and growth of aragonite platelets [11] but also serves as a glue to keep the integrity of the nacre structure [12]. Biopolymer between the aragonite nanoparticles allows the spacing and rotation of these nanoparticles and thus the inelastic deformation and toughening of nacre [10]. Having a specific modular structure, the biopolymer molecule in nacre matrix can unfold and refold its modular domains and dissipate

more energy during deformation [13], which also contributes to the strengthening and toughening of nacre.

Since biopolymer matrix plays a key role in the strengthening and toughening of nacre, considerable effort has been made to determine the mechanical properties of the biopolymer matrix of nacre [17-21]. Three dimensional finite element modeling of tensile test of nacre shows that the average elastic modulus of the biopolymer layer in nacre should be of the order of 15 GPa so that a realistic elastic modulus for the modeled nacre structure can be achieved [17]. Two dimensional finite element model of indentation on layered structure with 450-nm-thick tablets and 35-nm-thick interface was built to fit the experimental nanoindentation load-penetration depth curves of nacre and the best fit gives an elastic modulus of 2.84 ± 0.27 GPa for the biopolymer interfaces [18]. Through both shallow and deep Hertzian indentation on nacre, elastic modulus of the “intercrystalline” organic phase was also drawn from a structure model using the relationship of the transversal Young’s modulus of a stacking of layers made up of pure matrix and reinforced layers (biopolymer and aragonite). The elastic modulus so determined is 6.308 GPa for the biopolymer matrix, which is about one tenth of the aragonite [19]. Recently, combining Hertzian and Berkovich indentations of nacre and the Mori-Tanaka’s model for composite elastic modulus calculation, an elastic modulus of 3.81 GPa was obtained for the biopolymer matrix [20]. Using elastic modulus mapping technique and finite element simulation, the elastic modulus of biopolymer matrix of Perna canaliculus shells (mainly beta-chitin) is estimated to be 40 GPa [21]. However, due to the dimensional limitation of the biopolymer matrix (layer thickness less than 30 nm), all the above measurements of elastic modulus with a wide variation from 2.84 to 40 GPa are indirect and inevitably affected by the nearby aragonite platelets.

In this study, a novel approach combining direct AFM probing of biopolymer strands and inverse finite element analysis was used to determine the elastic modulus of nacre biopolymer matrix. Bending test was directly performed on the biopolymer strands formed in the tensile stress field of a notched beam subjected to three-point bending using atomic force microscopy (AFM). Cantilever position and deflection curves of the bending test of biopolymer strands were obtained using AFM. Inverse finite element analysis was resorted to determine the elastic modulus of biopolymer matrix by simulating the elastic bending of the biopolymer strands.

2. Experimental

2.1 AFM bending test of biopolymer strands

The nacre materials used in this study are from California red abalone (*Haliotis rufescens*) that belongs to the class of gastropoda. The shells were collected alive in Santa Barbara, CA. To minimize the detrimental effect of drying on the structure of shells, they were cleaned and air delivered in ice to the laboratory where the experiments were conducted. A notched beam specimen with dimension of 15 x 2.3 x 1.7 mm (length x height x width) was cut from the nacre layer of the shells with a water-cooled, low-speed diamond saw and the top surface of the specimen was mechanically ground and polished using abrasives and powders down to 50 nm in size. The specimen was then mounted to a custom-designed micromechanical tester which was integrated with a Dimension 3100 AFM (Veeco Metrology Group, Santa Barbara, CA) to perform three-point bending test while AFM imaging was carried out simultaneously around the notch tip, where stress concentration occurred and nacre material was mainly subjected to tensile stresses (Fig. 1a). Upon tension, the nacre material around the notch tip was deformed and

elongated and the biopolymer matrix between aragonite platelets was stretched to form the biopolymer strands as shown in Fig. 1b. The fractured nacre specimens were observed using a field emission scanning electron microscope (FE-SEM, Ultra Plus, Carl Zeiss SMT Inc., Peabody, MA) with an accelerating voltage of 5 kV. The SEM images (Fig. 1c) also show the biopolymer strands between the aragonite platelets.

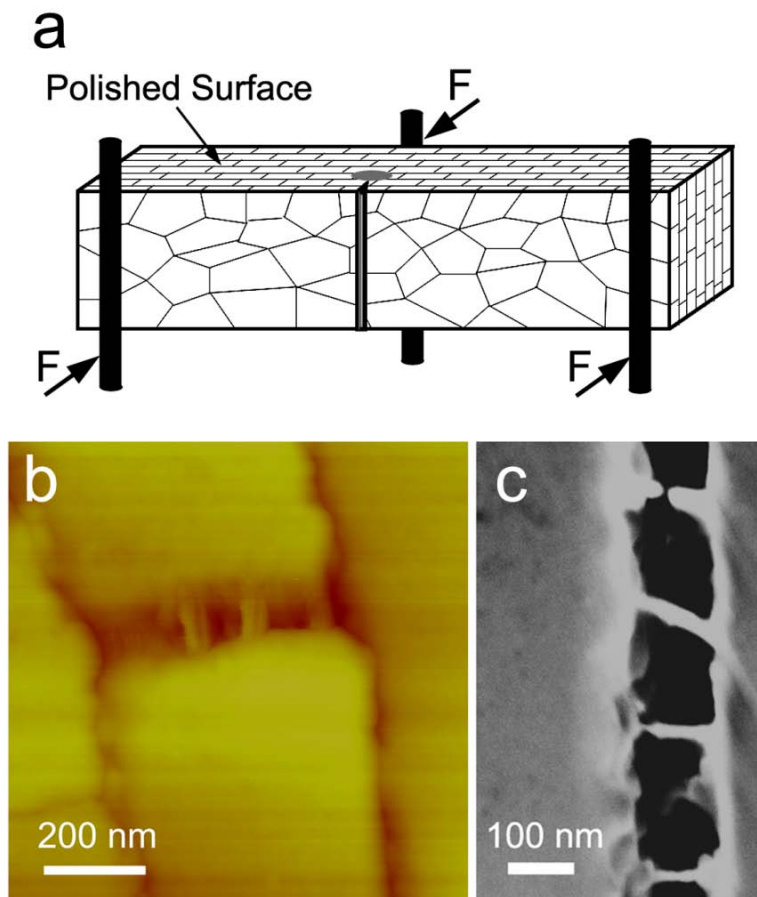


Fig. 1. (a) Schematic of three-point bending of notched nacre beam. (b) AFM image of the biopolymer strands formed between aragonite platelets in the tensile region of notched nacre beam. (c) SEM image of the biopolymer strands formed between aragonite platelets in the fractured nacre beam.

After the biopolymer matrix was stretched to form the biopolymer strands, a RESEP tapping AFM tip was used to perform a bending test at the middle of the biopolymer strand as schematically shown in Fig. 2a. During bending test, the AFM tip approached to the biopolymer strand at a velocity of 144nm/s. Once the AFM tip was in contact with the biopolymer strand, the cantilever started to deflect up and a bending force was applied to the biopolymer strand, which results in the deformation of the biopolymer. As shown in Fig. 2b, the relation between cantilever position, z , the deflection of cantilever, d_c , and the deformation of the biopolymer strand, d_s is given by

$$z = d_c + d_s \quad (1)$$

After the cantilever deflection reached a preset threshold, it will withdraw completely at the velocity of 144 nm/s.

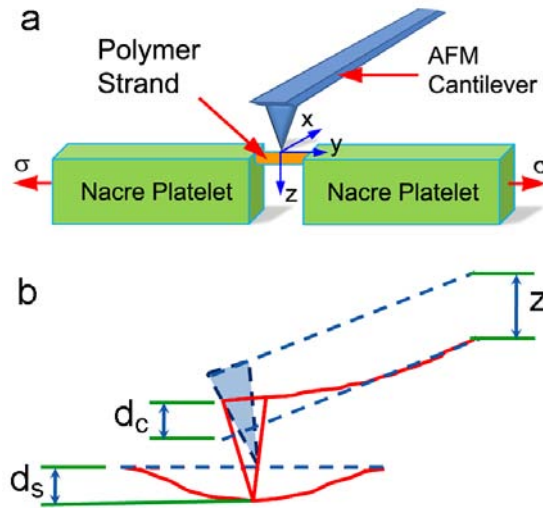


Fig. 2. (a) schematic of bending test directly performed on biopolymer strand using AFM tip. (b) Relationship between the cantilever z position, the cantilever deflection, and the deformation of the sample.

2.2 Modulus mapping test

Modulus mapping was also performed on the polished nacre surface to quantify the elastic modulus of the biopolymer interface between two aragonite platelets. The mapping was done with a 60° conical diamond indenter using Hysitron Triboscope (Hysitron Inc., Minneapolis, MN). During modulus mapping, a SR830 DSP Lock-in Amplifier (Stanford Research Systems Inc., Sunnyvale, CA) is used to apply a sinusoidal dynamic force with a frequency of 200 Hz additionally to the indenter tip which scans the sample surface with a constant force and the resultant sample displacement is recorded by the nanoindenter transducer. The oscillated dynamic force and resultant displacement can be used to calculate the contact stiffness and thus the elastic modulus with known indenter geometry.

3. Inverse finite element analysis

The initial bending of the biopolymer strands is mainly elastic deformation and can be used to determine the elastic modulus of the biopolymer matrix. This requires an inverse finite element analysis, that is, varying the input elastic properties of the biopolymer in a finite element model and getting an output cantilever position and deflection curve which best fits an individual experimental curve. A typical three dimensional finite element model used in this study is shown in Fig. 3. Considering the symmetry in y direction (see Fig. 2a), only half of the cantilever, the tip and the biopolymer strand was modeled. Very fine mesh was employed in the contact region of the tip and the biopolymer strand to insure convergence and accuracy of the simulation. The silicon tip was simplified as a cone with 20 ° half tip angle and tip radius of 10 nm. The average nominal height of the tip is 17.5 μm. The elastic modulus for the Si tip is 125 GPa [22]. The

cantilever beam normally has a gold top layer to reflect the laser to a photodiode detector to control either a constant contact or tapping force between tip and sample surface. The effective elastic modulus E_c of the cantilever for finite element modeling is determined using the following equation [23]

$$E_c = \frac{2ka^2(3L-a)}{wt^3} \quad (2)$$

where k is the spring constant of the cantilever beam, $k=34.4$ N/m; a is distance between the center of the tip to the end of the cantilever beam, $a=120.68$ μm [24]; L , w , and t are the length, width, and thickness of the cantilever beam (as shown in Fig. 3) and $L=128$ μm , $w=35$ μm , and $t=4$ μm . This gives an effective elastic modulus of the cantilever beam 117.79 GPa. The dimension parameters of the biopolymer strands namely length and diameter were measured directly from the AFM images. Detailed dimension of the five biopolymer strands for the bending test is listed in Table 1. The Poisson's ratio used for the tip and the cantilever beam is 0.25 while Poisson's ratio for the biopolymer is 0.3.

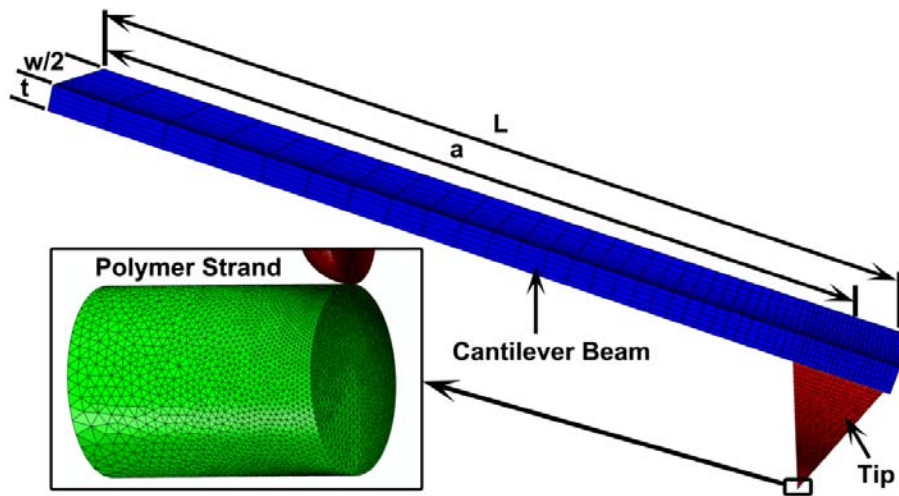


Fig. 3. Finite element model of the bending test of biopolymer strand.

The following boundary conditions were used in the finite element model. Roller boundary conditions were applied to the nodes on the y axis-symmetry planes of the cantilever, tip, and the biopolymer strand. Nodes on the end of biopolymer strand in contact with aragonite platelet were pinned during the simulation. Bending of the biopolymer was performed by stepwise applying a 5 nm displacement in z direction at the end of the cantilever beam and the corresponding deflection of the cantilever beam was determined at the node on top of the cantilever beam that coincides with the axis of the conical tip. No friction was considered between the tip and the biopolymer strand.

4. Results and discussion

4.1 Elastic modulus mapping of interface between aragonite platelets

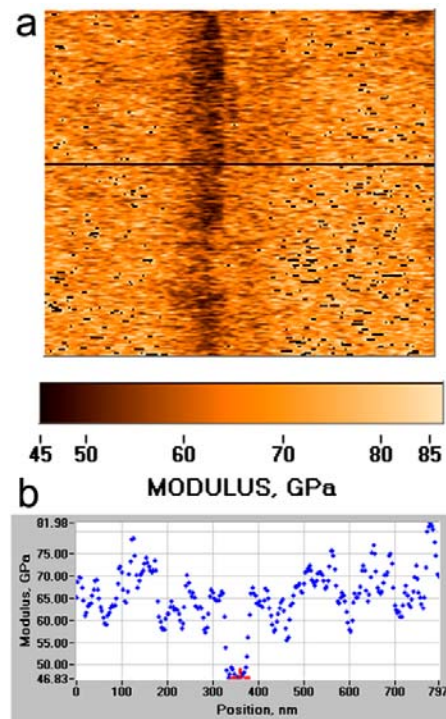


Fig. 4. Modulus mapping of biopolymer interface. (a) Elastic modulus map in a 800x800 nm area covering the biopolymer interface. (b) Modulus variation along the solid line shown in (a).

Fig. 4 shows the elastic modulus mapping of an interface layer between two aragonite platelets. As shown in Fig. 4a, the measured elastic modulus of the aragonite platelets (bright) is much higher modulus than the interface (dark). This modulus difference can be clearly seen in Fig. 4b where the variation of elastic modulus along the solid line in Fig. 2a is plotted. The elastic modulus of aragonite platelet reported in the literature [1,9,25-30] is in the range of 50 to 100 GPa with a commonly accepted value about 70 GPa. By varying the indenter tip radius for modulus mapping, the elastic modulus of aragonite platelets shown in Fig. 4 has been adjusted to the value around 70 GPa. A randomly selected 20 values inside each platelet give an average elastic modulus of 68.81 ± 6.91 GPa for aragonite platelet while a randomly selected 40 values within the interface give an average elastic modulus of 48.81 ± 2.51 GPa for the biopolymer. This value is a bit higher than 40 GPa [21] obtained combining a similar modulus mapping technique and finite element simulation. However, the ratio of elastic modulus of the aragonite to the biopolymer is 0.71, which agrees well with the normalized elastic modulus of the biopolymer interface experimentally measured by modulus mapping [21]. Although the elastic modulus mapping technique provides insightful information of the modulus variation across the biopolymer interlayer, due to the physical dimension of the indenter tip and very narrow biopolymer thickness, it is impossible to eliminate the effect of nearby aragonite platelets. Therefore, a more realistic modulus value of the biopolymer matrix, which is still absent in the literature, should be determined by directly probe the biopolymer strands without the influence from nearby aragonite platelets.

4.2 AFM bending test of biopolymer strands

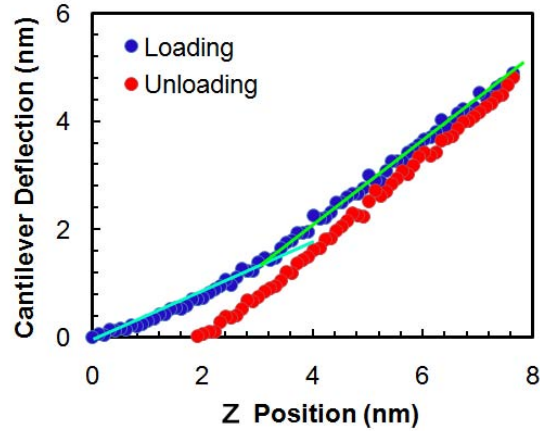


Fig. 5. Typical AFM cantilever z position and deflection curve for bending of biopolymer strand.

A typical AFM cantilever z position-deflection curve of bending test of biopolymer strand is shown in Fig. 5. The curve consists of two parts, the loading and the unloading segments. The loading segment shows a bilinear trend with the initial slope smaller than the final one indicating a strengthening behavior during the bending deformation. The initial linear loading curve is mainly dominated by elastic bending deformation while inelastic deformation occurs during the final stage of loading. The transition from elastic and inelastic bending behavior occurs around a cantilever position $z = 3\text{nm}$. The unloading segment deviates from the loading one confirming the inelastic deformation of the biopolymer strand during bending. The strengthening behavior of the biopolymer matrix during bending can be explained by the unfolding of the modular structure of biopolymer molecules and a physical coil spring model. Detailed discussion and explanation about of the deformation behavior during bending and the strengthening mechanism of the nacre biopolymer matrix will be presented elsewhere.

4.3 Inverse finite element analysis

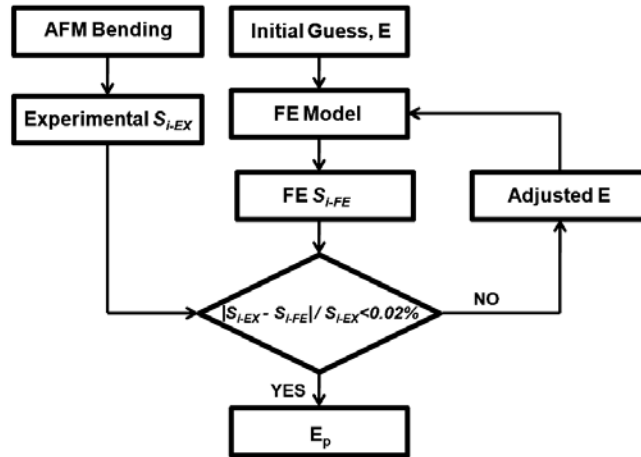


Fig. 6. Flow chart of the inverse analysis procedure for the elastic modulus determination of biopolymer strands.

The flow chart for inverse finite element analysis is shown in Fig. 6. To determine the elastic modulus of the biopolymer matrix of nacre, an initial guess elastic modulus E is first input into the finite element model. Simulation of bending test is then carried out numerically to obtain the cantilever z position and deflection curve and a slope of the z position and deflection curve at the initial 3 nm movement of the cantilever S_{i-FE} is determined. Then the S_{i-FE} is compared to the experimentally measured S_{i-EX} . If the difference between S_{i-EX} and S_{i-FE} is larger than 0.02% of S_{i-EX} , the input E will be adjusted and finite element simulation will run again to determine the S_{i-FE} . This iteration will be repeated until the elastic modulus of biopolymer, E_p , which gives an error between S_{i-EX} and S_{i-FE} less than 0.02%, is obtained.

Fig. 7 shows the comparison of the cantilever z position and deflection curves of finite element analysis (FE) and experimental AFM bending test (EX) for five biopolymer strands. As can be seen, very good agreement between finite element analysis and experimental AFM bending has

been achieved, which in turn leads to an excellent agreement of the slopes of the z position and deflection curves between finite element simulations and experiments as shown in Table 1. The elastic modulus determined from the inverse finite element analysis of each biopolymer strand is also listed in Table 1. The elastic moduli of biopolymer strands range from 7.67 GPa to 13.74 GPa with an average value of 10.57 GPa and a standard deviation of 2.56 GPa. This property is essential for a fundamental understanding of the roles that the biopolymer matrix plays in nacre's strengthening and toughening, and provides guidelines in selecting engineering polymers for biomimetic materials design and fabrication.

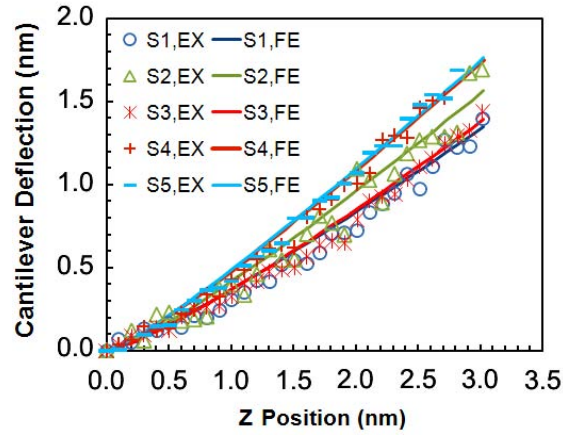


Fig. 7. Comparison of the AFM cantilever z position and deflection curves of biopolymer strands obtained from finite element simulations and experimental bending tests.

Table 1. Dimension and elastic modulus of biopolymer strands

Biopolymer Strand	Dimension		Initial Slope		E (GPa)
	Length (nm)	Diameter (nm)	S_{i-EX}	S_{i-FE}	
S1	100	36	0.4504	0.4504	9.75
S2	108	62	0.5222	0.5222	8.97
S3	125	55	0.4644	0.4644	7.67
S4	118	67	0.5858	0.5859	12.72
S5	129	63	0.5884	0.5885	13.74

5. Conclusions

A novel approach combining direct AFM probing of nacre biopolymer strand and inverse finite element analysis was used to determine the elastic modulus of nacre biopolymer matrix. The elastic modulus so determined for nacre biopolymer matrix without the nearby aragonite platelet influence is 10.57 ± 2.56 GPa. This information will be helpful for understanding and modeling of deformation behavior and fracture of nacre and related biomaterials. The combined AFM probing and inverse finite element analysis techniques are unique and should find more applications in studying the mechanical behavior of other biomaterials.

Acknowledgments

This work was supported by the U.S. Army Research Office under agreement/grant No. W911 NF-07-1-0449. We thank R. Z. Wang for providing the nacre samples.

References

- [1] A.P. Jackson, J.F. Vincent, R.M. Turner. Proc. R. Soc. London Ser. B 234 (1988) 415.
- [2] J.D. Curry. Proc. R. Soc. London Ser. B 196 (1997) 443.
- [3] X.D. Li, W.C. Chang, Y.J. Chao, R.Z. Wang, M. Chang. Nano Lett. 4 (2004) 613.
- [4] S. Kamat, X. Su, R. Ballarini, A.H. Heuer. Nature 405 (2000) 1036.
- [5] A.G. Evans, Z. Suo, R.Z. Wang, I.A. Aksay, M.Y. He, J.W. Hutchinson. J. Mater. Res. 16 (2001) 2475.
- [6] R.Z. Wang, Z. Suo, A.G. Evans, N. Yao, I.A. Aksay. J. Mater. Res. 16 (2001) 2485.
- [7] K.S. Katti, D.R. Katti, S.M. Pradhan, A. Bhosle. J. Mater. Res. 21 (2006) 1237.
- [8] F. Barthelat, H. Tang, P.D. Zavattieri, C.M. Li, H.D. Espinosa. J. Mech. Phys. Solids 55 (2007) 306.
- [9] F. Song, A.K. Soh, Y.L. Bai. Biomater. 24 (2003) 3623.
- [10] X.D. Li, Z.H. Xu, R.Z. Wang. Nano Lett. 6 (2006) 2301.
- [11] M.A. Meyers, C.T. Lim, A. Li, B.R. Hairul Nizam, E.P.S. Tan, Y. Seki, J. McKittrick. Mater. Sci. Eng. C 29 (2009) 2398.
- [12] M.A. Meyers, A.Y.M. Lin, P.Y. Chen, J. Muiyco. J. Mech. Behav. Biomed. Mater. 1 (2008) 76.
- [13] B.L. Smith, T.E. Schaffer, M. Viani, J.B. Thompson, N.A. Frederick, J. Kindt, A. Belcher, D. Stucky, D.E. Morse, P.K. Hansma. Nature 399 (1999) 761.
- [14] A. Sellinger, P.M. Weiss, A. Nguyen, Y. Lu, R.A. Assink, W. Gong, J. Brinker. Nature 394 (1998) 252.
- [15] Z.Y. Tang, N.A. Kotov, S. Magonov, B. Ozturk. Nature Mater. 2 (2003) 413.
- [16] C. Ortiz, M.C. Boyce. Science 319 (2008) 1053.

- [17] D.R. Katti, K.S. Katti. *J. Mater. Sci.* 36 (2001) 1411.
- [18] F. Barthelat, C.M. Li, C. Comi, H.D. Espinosa. *J. Mater. Res.* 21 (2006) 1977.
- [19] Ph. Stempfle, O. Pantale, R. Kouitat Njiwa, M. Rousseau, E. Lopez, X. Bourrat. *Int. J. Nanotechnol.* 4 (2007) 712.
- [20] Ph. Stempfle, O. Pantale, M. Rousseau, E. Lopez, X. Bourrat. *Mater. Sci. Eng. C* 30 (2010) 715.
- [21] H. Moshe-Drezner, D. Shilo, A. Dorogoy, E. Zolotoyabko. *Adv. Funct. Mater.* 20 (2010) 2723.
- [22] Z.H. Xu, Y.B. Park, X.D. Li. *J. Mater. Res.* 25 (2010) 880.
- [23] T.J. Lardner. *An Introduction to the Mechanics of Solids.* Now York, McGraw-Hill, 1972.
- [24] Z.H. Xu, M.A. Sutton, X.D. Li. *Acta Mater.* 56 (2008) 6304.
- [25] R. Menig, M.H. Meyers, M.A. Meyers, K.S. Vecchio. *Acta Mater.* 48 (2000) 2383.
- [26] F.D. Fleischli, M. Dietiker, D. Borgia, R. Spolenak. *Acta Biomater.* 4 (2008) 1694.
- [27] B.H. Ji, H.J. Gao. *J. Mech. Phys. Solids* 52 (2004) 1963.
- [28] R.Z. Wang, Z.G. Suo, N. Yao, I.A. Aksay. *J. Mater. Res.* 15 (2001) 2485.
- [29] K.S. Katti, B. Mohanty, D.R. Katti. *J. Mater. Res.* 21 (2006) 1237.
- [30] B.J.F. Bruet, H.J. Qi, M.C. Boyce, R. Panas, K. Tai, C. Ortiz. *J. Mater. Res.* 20 (2005) 2400.

New deformation mechanism in nacre

Zaiwang Huang¹, Haoze Li¹, Zhiliang Pan², Qiuming Wei², Xiaodong Li^{1*}

¹ Department of Mechanical Engineering, University of South Carolina, 300 Main Street, Columbia, South Carolina 29208, USA.

² Department of Mechanical Engineering, University of North Carolina at Charlotte, 362, ERB, Charlotte, NC 28223, USA.

Under high strain rate ($\sim 10^3 \text{ s}^{-1}$) compression, nacre exhibits surprisingly high fracture strength and relatively marked plastic deformation excursion compared with those in the quasi-static (10^{-3} s^{-1}) loading mode, nevertheless the mechanism at work within nacre why they behave so distinctly in these two loading modes remains completely unknown. Here we report a new deformation mechanism, adopted by natural nacre to protect from predatory penetrating impacts, that the emission of partial dislocation and the onset of deformation twinning jointly contribute a dominated role in the increased fracture strength and ductility. Our findings have provided solid evidence that Mother Nature delicately use design principle down to atomic scale with a purpose to fight against foreign attacks, which has opened up a new opportunity to unravel the deformation mechanism of unique mechanical performance at the atomic scale.

* Corresponding author.

lixiao@cec.sc.edu

<http://www.me.sc.edu/research/nano/>

Nacre has attracted huge attention in the past decades and is long renowned for the natural armor materials with superior mechanical strength and toughness [1~11]. It is a nanocomposite with highly organized polygonal aragonite (A polymorph of CaCO_3) platelet of 200~500 nm thickness sandwiched by biopolymer interlay with a thickness ranging from 5 to 20 nm. Such an ingenious assembly principle makes nanocomposite nacre achieve remarkable improvement with two fold increase in strength and 1000 fold increase in toughness comparing with its counterpart. Several deformation mechanisms, such as crack deflection [3], interlocking [11], nanoasperities [5], mineral bridge [2, 7], are believed to collectively contribute to nacre's mechanical robustness. However, the nacre's basic building block, individual aragonite platelets, receives less attention for its role and working mechanism during deformation. Recent work shows that single aragonite platelet is essentially composed of nanograins with parallel crystallographic orientation [13-15]. In situ Atomic Force Microscope observation indicates that individual aragonite platelets are not brittle, but deformable due to nanograins rotation and plastic deformation [16]. Nevertheless, in fact, a key question we need to answer is that how natural nacre protects itself when suffering from a high speed predatory penetrating attack [12], Will the protect mechanism nacre use under shock load be same with that we have explored using conventional testing methods in quasi-static

mode? To unveil the mechanism, the knowledge of structure-property relationships under shock is in need for in-depth understanding. In this letter, we design a group of compression experiments at shock and quasi-static loading mode. We propose shock compression at a high strain rate ($\sim 10^3 \text{ s}^{-1}$) with a purpose to mimic predatory penetrating impacts (typically $10^2 \sim 10^3 \text{ s}^{-1}$) red abalone undergo in actual existence environment in sea. We find, comparing with those in quasi-static load, that nacre can resist much higher shock compressive stress and reveal more superior plasticity deformation capability through the emission of partial dislocation and the onset of deformation twinning, which are related to the combined factors of high strain rate and nanometer-size confinement.

Natural red abalone nacre (*Haliotis rufescens*) alive, which were collected in Santa Barbara beach, CA, belong to the class of gastropoda. They were air delivered with ice to the laboratory for the consideration to reduce the detrimental effect of drying. Nacre compression samples were cut from the nacreous layer with a water-cooled, low-speed diamond saw. The quasi-static and shock compression test are respectively carried out by the Instron 5566 and Kolsky (or Split Hopkinson pressure (SHPB)) bar system [17,18], where the nacre samples are sandwiched between the input and output bars. For simplicity, we only test the rectangular samples

compressed along cross section direction. The post-mortem powder samples were directly collected and dispersed into distilled water using ultrasonic wave for two hours. The TEM powder samples were transferred onto the holey carbon-coated copper film for observation in a JEOL JEM 2100F transmission electron microscope at an accelerating voltage of 200 KV.

True stress-strain curves (Figure.1) reveal compression behavior under dynamic and quasi-static loading. In the case of quasi-static mode, the fracture stresses measured from four lower curves (dot lines) are arranged 80-200 MPa, and true strains are generally lower than 4%. In contrast, the peak stresses loaded from dynamic compression (solid lines) are typically in the range of 450-500 MPa, which is 2~3 times for the corresponding values in quasi-static tests. In addition, the true strains associated with plasticity deformation capability prevalently reach a level 4% to 6%, which have obviously been improved with the dynamic background.

Based on above distinct results, a question is raised to be answered: what role do nacre's aragonite platelets play and how do they work? HRTEM observations (Figure 2A) indicated that, when deformed in quasi-static load, aragonite platelet consisted of irregular-shaped nanograins with random orientations. A smaller box area (blue box in Figure 2(A)) with

interest was chosen to present a closer-view of lattice fringe details. Analysis on boxed area showed that at least four nanograins were incorporated and remained random orientation (Figure 2(B)). We suggested, for the first time, that nanograins in a parallel manner rotated and plastically deformed, corresponding to the feature from Fast Fourier Transform (FFT) pattern (Figure 2(C)).

Nevertheless, what was picture within single aragonite platelet under shock compression? HRTEM image (Figure 3(A)) showed nanometer-sized deformation zone composing of nanograins with random orientation, which scattered like ring pattern (inset). Accordingly, a closer-up examination on white-boxed area showed that lattice irregularities were triggered in nanometer-sized grain through the atomic measurement and analysis (Figure 3(B), which could be identified as partial dislocation, a new crystallographic defect never seen in nacre. The atomic details indicated that the regular sequence of atoms terminated at the site (red arrowed) and atoms (white arrowed) slid to crystallographic plane by introduction of a Burgers Vector \vec{b}_1 , which could be visualized as partial dislocation by $\left| \vec{b}_1 \right| \langle \left| \vec{b}_2 \right|$, Figure 3(C) was a schematic illustration exhibiting how partial dislocations were recognized via measuring atomic spacing, where \vec{b}_2 represented a unit cell vector in aragonite, the magnitude of which equals to a integer atomic spacing.

Previous results showed that both microstructure change [19] and external load [20] could trigger deformation twinning, which was not prevalent in conventional crystalline solid. The deformation twinning (Figure 1(A)) can be identified by the mirror symmetry between matrix and twin with atomic resolution image together with FFT pattern (inset), which scattered dual-spot pattern. A closer-up view on matrix-twin boundary indicated that twin boundaries (TB) were atomically sharp, but not perfectly coherent, which was indexed as (110) plane (Figure 4(B)). Combined with atomic image and FFT pattern (Figure 4(C)), twin was determined to occur on the (110) plane. Our previous experimental results show that individual platelets are essentially composed of nanograins with a few to tens of nanometers [13-16]. We suggest that shock impact combined with such a size regime (several to tens of nanometers) in aragonite crystal can restrain full dislocations activities, and partial dislocations take a dominated effect on plastic deformation. However, the formation mechanism of deformation twinning is an open question to be answered.

What will happen at grain boundary between aragonite nanograins? Our previous TEM results [14] show that there exist at least two types of imperfect transition: screw dislocation and amorphous aggregation. Figure 4(A) exhibit the offspring of amorphous aggregation surrounded

by nanograins after shock compression. The messy spot diffraction pattern (inset) indicates that ordered arrangements of aragonite nanograins have been broken after deformation. Our observation reversely confirms our assumption [14] that amorphous aggregation is an important transition phase as grain boundary between nanograins.

In summary, we firstly demonstrate solid evidence that two new deformation mechanisms, involving partial dislocation and deformation twinning, are triggered in individual aragonite platelet of nacre under shock attack. The high shock stress and more superior ductibility benefit for nacre's protection from predatory penetrating impact. Based on the observation, our results firmly confirm the fact that individual platelets are essentially composed of aragonite nanograins.

References

1. A. P. Jackson, J. F. V. Vincent, R. M. Turner, *Proc. R. Soc. London Ser. B.* **234**, 415 (1988).
2. T. E. Schaffer, et al. *Chem Mater*, **9**, 1731 (1997).
3. Q. L. Feng, F. Z. Cui, G. Pu, R. Z. Wang, H. D. Li, *Mater. Sci. Eng. C.* **11**, 19 (2000).
4. R. Menig, M. H. Meyers, M. A. Meyers, K. S. Vecchio, *Acta Mater.* **48**, 2383 (2000).
5. R. Z. Wang, Z. G. Suo, A. G. Evans, N. Yao, I. A. Aksay. *J. Mater. Res.* **16**, 2485 (2001).

6. H. J. Gao, B. H. Ji, I. L. Jager, E. Arzt, P. Fratzl, *Proc. Natl. Sci. U.S.A.* **100**, 5597 (2003).
7. F. Song, A. K. Soh, Y. L. Bai, *Biomaterials*, **24**, 3623 (2003).
8. N. Nassif, N. Pinna, N. Gehrke, M. Antonietti, C. Jager, and H. Colfen, *Proc. Natl. Acad. Sci. U.S.A.* **102**, 12653 (2005)
9. M. Rousseaua, E. Lopeza, P. Stempfle, M. Brendle, L. Franked, A. Guetted, R. Naslained, X. Bourrat, *Biomaterials*, **26**, 6254 (2005).
10. F. Barthelat, C. M. Li, C. Comi, H. D. Espinosa, *J. Mater. Res.* **21**, 1977 (2006).
11. S. K. Katti, B. Mohanty, D. R. Katti, *J. Mater. Res.* **21**, 1237 (2006).
12. C. Ortiz, M.C. Boyce, *Science*, **319**, 1053 (2008).
13. X. D. Li, W. C. Chang, Y. J. Chao, R. Z. Wang, M. Chang, *Nano Letters*, **4**, 613 (2004).
14. X. D. Li, Z. W. Huang, *Phys. Rev. Lett.* **102**, 975502 (2009).
15. Z. W. Huang, X. D. Li, *Mater. Sci. Eng. C.* **29**, 1803 (2009).
16. X. D. Li, Z. H. Xu, R. Z. Wang, *Nano letters*, **6**, 2301 (2006).
17. Q. Wei, H. T. Zhang, B. E. Schuster, K. T. Ramesh, R. Z. Valiev, L. J. Kecskes, R. J. Dowding, L. Magness, K. Cho. *Acta Mater.* **54**, 4079 (2006).
18. Q. Wei, T. Jiao, K. T. Ramesh, E. Ma, L. J. Kecsckes, L. J. Kecskes, R. Dowding . V. U. Kazykhanov, R. Z. Valiev. *Acta Mater.* **54**, 77 (2006).
19. M. Chen, E. Ma, K. J. Hemker, H. W. Sheng, Y. M. Wang. X. M. Cheng, *Science.* **300**, 1275 (2003).
20. V. Yamakov, D. Wolf, S. R. Phillpot, A. K. Mukherjee, H. Gleiter, *Nature Mater.* **1**, 45(2002).

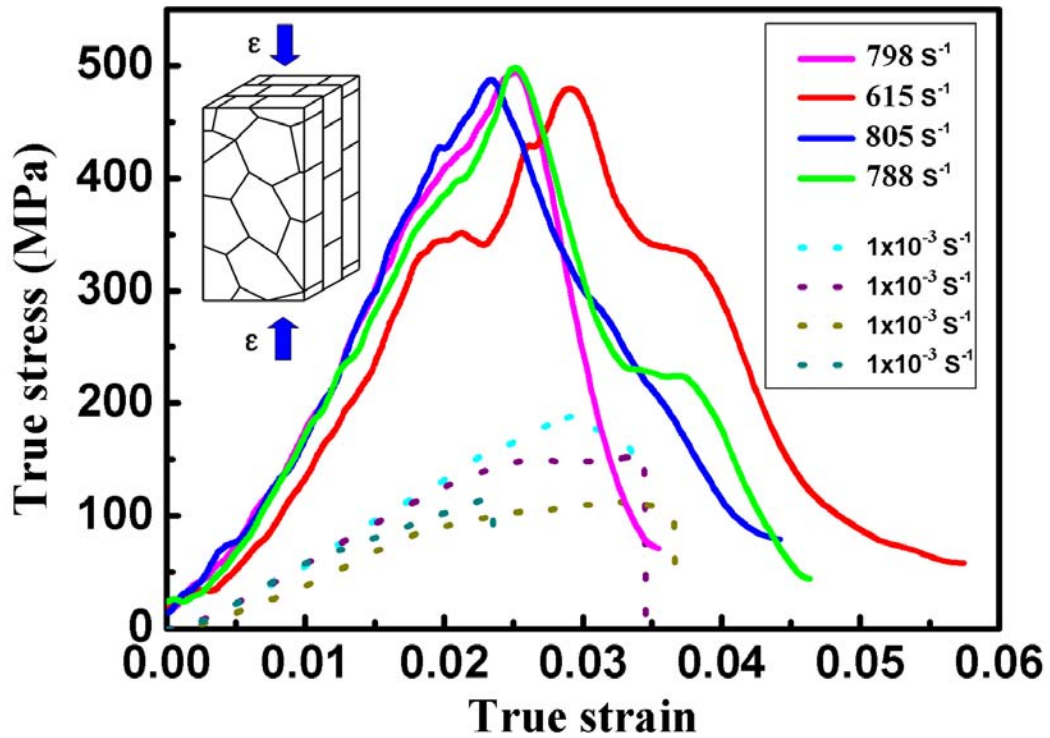


Fig.1. The true stress-strain behavior of nacre under shock ($\sim 10^3 \text{ s}^{-1}$) and quasi-static compression (10^{-3} s^{-1}). The stress-strain curves shows that maximal compressive stresses in shock are typically as high as 500 MPa, far exceeding those (generally below 200 MPa) in quasi-static mode, and the plastic deformation capability has been improved markedly.

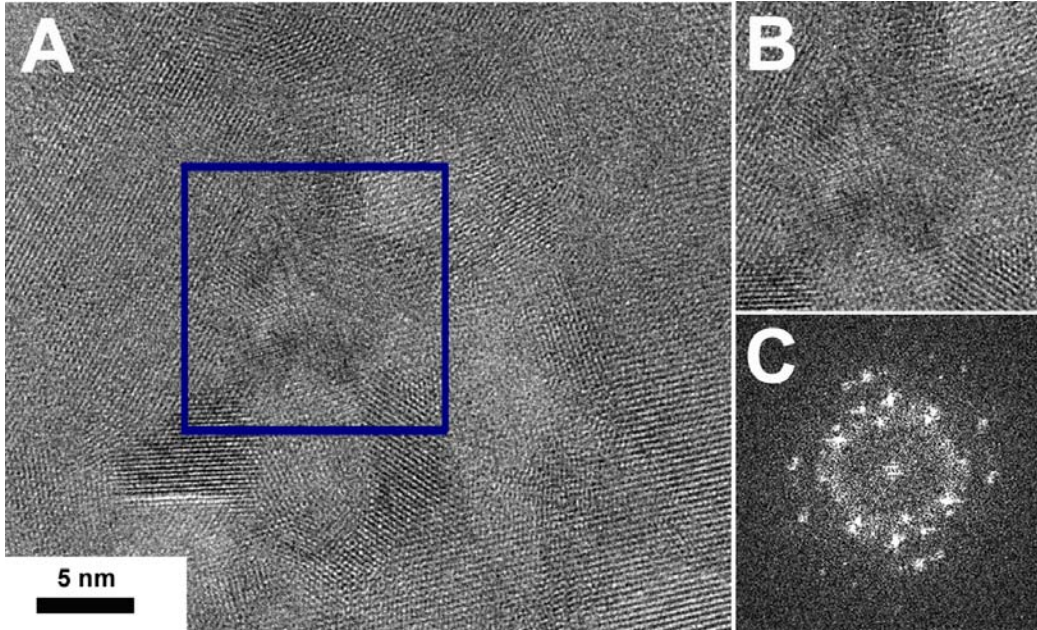


Fig. 2. Disordered aragonite nanograins. When deformed, nanograins, rearranged in a disorganized manner (A), a closer-view on blue box shows that at least four nanograins with random orientation pile up at this area (B), where the FFT scatters a messy-spot pattern (C).

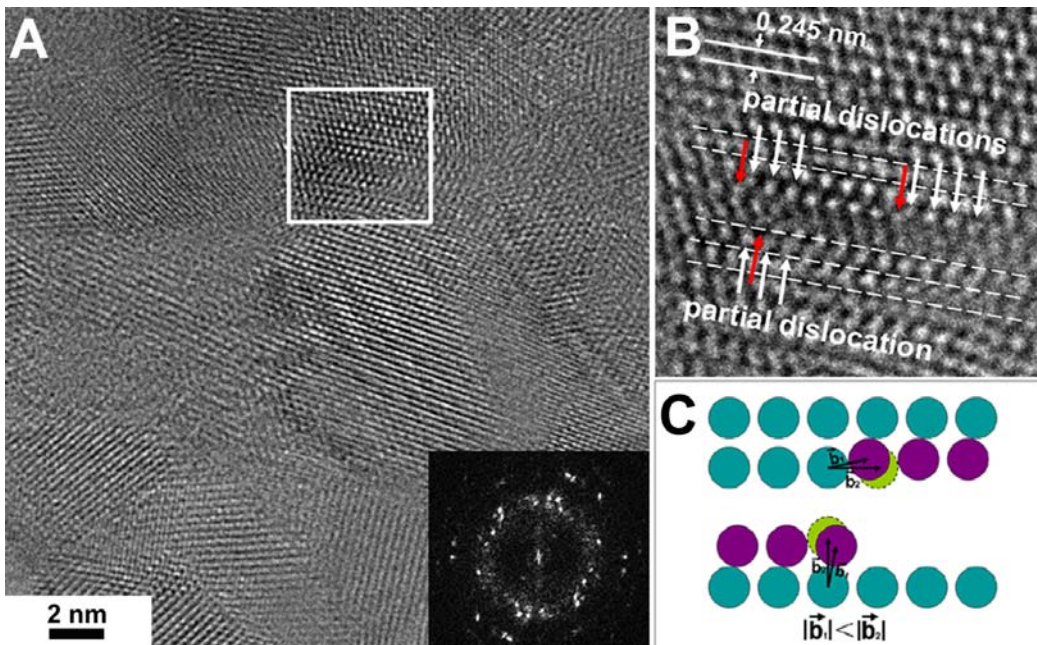


Fig. 3. Analysis and confirmation of partial dislocation. The region with disordered nanograins (A) scatters ring-like pattern (inset), indicating that a process involving grain boundary rotation has taken place. In detail, new crystallographic irregularity within one grain (white box) can be measured and analyzed with a point-to-point resolution (B), the partial dislocation can be determined by the characterization and measurement of burgers vector, which is schematically illustrated (C).

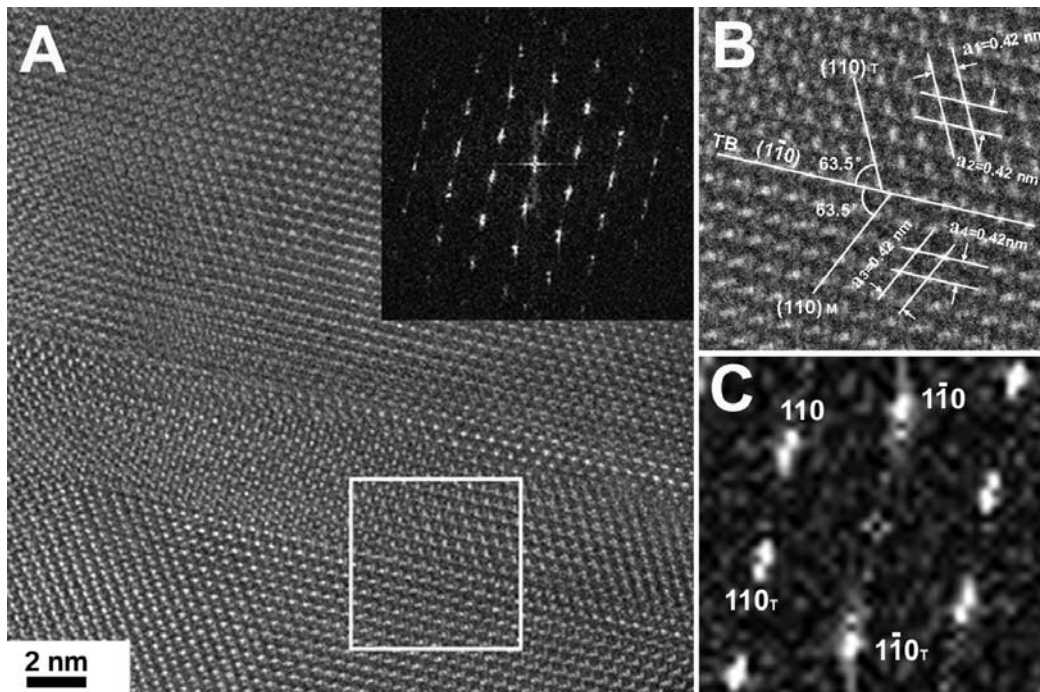


Fig. 4. (A) TEM micrograph of deformation twinning. The inset is the confirmation of twinning using FFT analysis. (B) A closer-up view on twinning boundary and its mirror symmetry relation from white boxed area. (C) The FFT showing the twinning relation between narrow band and matrix.

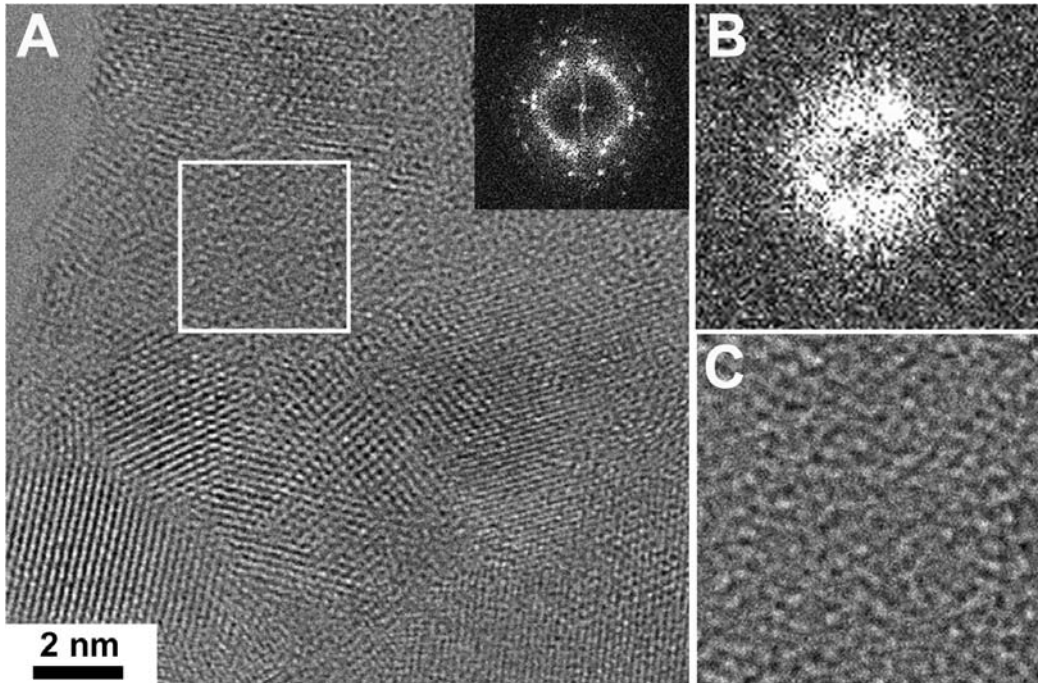


Fig. 5. TEM micrograph of amorphous aggregation. (A) amorphous aggregation are surrounded by nanometer-sized aragonite grains with random orientation characterized by FFT pattern (inset). (B) FFT without clear spot pattern from white boxed region shows a characteristic of amorphous aggregation. (C) A closer-up view of amorphous aggregation from corresponding white boxed area in (A) shows a mosaic feature.